EUROPEAN ORGANIZATION FOR NUCLEAR RESEARCH

CERN-EP-2024-271
15 October 2024

Measurements of differential two-particle number and transverse momentum correlation functions in pp collisions at $\sqrt{s}$ = 13 TeV

ALICE Collaboration*

Abstract

Differential two-particle normalized cumulants (R_2) and transverse momentum correlations (P_2) are measured as a function of the relative pseudorapidity and azimuthal angle difference $(\Delta\eta,\Delta\varphi)$ of charged particle pairs in minimum bias pp collisions at $\sqrt{s}$ = 13 TeV. The measurements use charged hadrons in the pseudorapidity region of $|\eta| < 0.8$ and the transverse momentum range $0.2 < p_{\mathrm{T}} < 2.0$ GeV/c in order to focus on soft multiparticle interactions and to complement prior measurements of these correlation functions in p–Pb and Pb–Pb collisions. The correlation functions are reported for both unlike-sign and like-sign pairs and their charge-independent and charge-dependent combinations. Both the R_2 and P_2 measured in pp collisions exhibit features qualitatively similar to those observed in p–Pb and Pb–Pb collisions. The $\Delta\eta$ and $\Delta\varphi$ root mean square widths of the near-side peak of the correlation functions are evaluated and compared with those observed in p–Pb and Pb–Pb collisions and show smooth evolution with the multiplicity of charged particles produced in the collision. The comparison of the measured correlation functions with predictions from PYTHIA8 shows that this model qualitatively captures their basic structure and characteristics but feature important differences. In addition, the R_2^{CD} is used to determine the charge balance function of hadrons produced within the detector acceptance of the measurements. The integral of the balance function is found to be compatible with those reported by a previous measurement in Pb–Pb collisions. These results, which are sensitive to the interplay between the underlying event and mini-jets in pp collisions, establish a baseline for heavy-ion collisions.

---

*See Appendix A for the list of collaboration members

1 Introduction

Understanding the mechanisms involved in the production of particles in collisions of heavy nuclei and their subsequent interactions in the medium created in the collision is an important aspect of the physics programs of the Relativistic Heavy Ion Collider (RHIC) and the Large Hadron Collider (LHC). Measurements carried out in the last two decades indicate that a new form of matter, consisting of deconfined quarks and gluons and known as quark–gluon plasma (QGP), is produced in collisions of large nuclei (e.g., Au and Pb) at the very high energies available at these facilities. Evidence for this new form of matter arises in part from measurements of nuclear modification factors which indicate that the matter produced in these collisions is rather opaque to the propagation of high momentum partons [1–10]. Also, observations of collective behavior suggest that the matter formed is strongly interacting and features a nearly vanishing specific shear viscosity [11–17].

Recently, there has been great interest in investigating whether such opaque matter can be produced in small collision systems, such as pp and p–Pb collisions. There are a variety of techniques used for such investigations, which include attempts to identify jet quenching relative to the system geometry and efforts to identify collective flow based on multiparticle correlations [18, 19]. In parallel with these investigations, it is also of interest to determine how the particle production evolves from small to large collision systems [20]. Transverse momentum spectra of produced particles are evidently a prime source of such information. However, it is also found that measurements of differential particle correlations bring additional information for the understanding of the production of hadrons and their interactions in small and large collision systems. Among these, measurements of number (R_2) and transverse momentum (P_2) two-particle correlation functions have been already explored in p–A and A–A collisions [21–23]. Furthermore, the measured balance function in pp, p–A, and A–A collisions as a function of multiplicity presents considerable challenges to the leading models used in heavy-ion physics [23]. It is thus of interest to find out whether measurements of these correlation functions in pp collisions can similarly challenge the leading models used towards the description of particle production in small systems.

Recent measurements of R_2 and P_2 have played an important role in independent verification of the collective nature of azimuthal correlations observed in Pb–Pb collisions [24, 25]. Both the R_2 and P_2 correlation functions are indeed sensitive to the presence of collectivity and may contribute to further elucidation of this phenomenon in small systems relative to that observed in larger systems [20, 26]. Moreover, prior measurements have also revealed distinct differences in the dependence on $\Delta\eta$ $(\equiv \eta_1 - \eta_2)$ and $\Delta\varphi$ $(\equiv \varphi_1 - \varphi_2)$, where η and φ are pseudorapidity and azimuthal angle of particles 1 and 2, for R_2 and P_2 correlation functions. The findings indicate that the near-side peak of both charge-independent (CI) and charge-dependent (CD) correlations in P_2 is notably narrower than in R_2, regardless of the centrality (collision impact parameter) [27] of Pb–Pb collisions [21]. This further supports the idea put forth in Ref. [28] that a comparative analysis of R_2 and P_2 correlation functions can offer increased sensitivity to the underlying mechanisms governing particle production in small as well as large collision systems.

The new measurements reported in this work are also designed to enable a better understanding of particle production processes underpinning the underlying event of pp collisions, and more specifically the particle production mechanisms involved in soft multiparticle production and the low transverse momentum components of jets [29]. Measurements in pp are also of interest to study the evolution of these correlation functions with the system size and their compatibility among the different collision systems at similar charged particle multiplicities. Thus, one of the main goals of this work is to provide additional information about the shape and magnitude of the correlation functions in the smallest hadronic collision systems. Consequently, this study is an important extension of recent measurements of these correlation functions in p–Pb and Pb–Pb collisions by the ALICE Collaboration [21]. The results involve measurements of the R_2 and P_2 correlation functions, and their characteristics, for CI and CD combinations of charged particles. These are compared with PYTHIA8 predictions to verify whether this model is capable of providing a reasonable description of correlated particle production in small collision systems.

Furthermore, inclusive charge balance function in pp collisions was measured. Charge balance functions have been exploited primarily in collisions of heavy nuclei to identify the presence of an extended period of isentropic expansion in these systems [23], but recent theoretical works also indicate that they enable the estimation of the diffusivity of light quarks and may also serve in the determination of QGP susceptibilities [30, 31].

This paper presents a comparative analysis of R_2 and P_2 correlation functions measured in pp collisions at a center-of-mass energy $\sqrt{s} = 13$ TeV. As in prior analyses of p–Pb and Pb–Pb collisions [21, 24], the two correlation functions are first measured for like-sign (LS) and unlike-sign (US) charged particle pairs. These are then combined to CI and CD correlation functions, as described in Sec. 2. These correlations are characterized by their azimuthal and longitudinal widths and compared with characteristics of R_2 and P_2 correlation functions measured in larger collision systems.

The article is organized as follows. The correlation functions, R_2 and P_2, and their LS, US, CI, and CD components are defined in Sec. 2. Section 3 presents a summary of the data taking conditions as well as the various technical details of the analysis, including event and track selection criteria, efficiency correction, quality tests, etc. The basic configuration of the Monte Carlo (MC) model used for quality control and towards the interpretation of the measured data is briefly described in Sec. 4. Section 5 presents a discussion of the techniques used for the estimation of the statistical and systematic uncertainties. The experimental results are presented in Sec. 6 where they are compared with PYTHIA8 predictions. A summary is provided in Sec. 7.

2 Definitions of observables

Particle number and transverse momentum correlations are reported based on R_2 and P_2 [28, 29] defined in terms of single- (ρ_1) and two-particle (ρ_2) densities

$$\rho_1(\eta_{\rm j},\varphi_{\rm j}) = \frac{{\rm d}^2N}{{\rm d}\eta_{\rm j}{\rm d}\varphi_{\rm j}}, \tag{1}$$

$$\rho_2(\eta_1,\varphi_1,\eta_2,\varphi_2) = \frac{{\rm d}^4N}{{\rm d}\eta_1{\rm d}\varphi_1{\rm d}\eta_2{\rm d}\varphi_2}, \tag{2}$$

where η_j, φ_j ($j = 1,2$) are the pseudorapidities and azimuthal angles of particles 1 and 2, respectively.

The number correlation function, R_2, is formulated as a two-particle cumulant normalized by the product of single-particle densities according to

$$R_2(\eta_1,\varphi_1,\eta_2,\varphi_2) = \frac{\rho_2(\eta_1,\varphi_1,\eta_2,\varphi_2)}{\rho_1(\eta_1,\varphi_1)\rho_1(\eta_2,\varphi_2)} - 1, \tag{3}$$

whereas the dimensionless transverse momentum correlation function, P_2, is defined as the ratio between $\langle\Delta p_{\rm T}\Delta p_{\rm T}\rangle$ and the square of the mean transverse momentum, $\langle p_{\rm T}\rangle$. This can be expressed as follows

$$P_2(\eta_1,\varphi_1,\eta_2,\varphi_2) = \frac{\langle\Delta p_{\rm T}\Delta p_{\rm T}\rangle(\eta_1,\varphi_1,\eta_2,\varphi_2)}{\langle p_{\rm T}\rangle^2}. \tag{4}$$

The $\langle\Delta p_{\rm T}\Delta p_{\rm T}\rangle$ differential correlation function is defined as

$$\langle\Delta p_{\rm T}\Delta p_{\rm T}\rangle(\eta_1,\varphi_1,\eta_2,\varphi_2) = \frac{\int_{p_{\rm T,min}}^{p_{\rm T,max}} \Delta p_{\rm T,1}\Delta p_{\rm T,2}\; \rho_2^{'}(\vec{p}_1,\vec{p}_2)\; {\rm d}p_{\rm T,1}{\rm d}p_{\rm T,2}}{\int_{p_{\rm T,min}}^{p_{\rm T,max}} \rho_2^{'}(\vec{p}_1,\vec{p}_2)\; {\rm d}p_{\rm T,1}{\rm d}p_{\rm T,2}}, \tag{5}$$

in which $\rho_2^{'}(\vec{p}_1,\vec{p}_2)$ is analogous for ρ_2, but is expressed as a function of the momenta $\vec{p}_1$ and $\vec{p}_2$ of the particles constituting the pair instead of their η and φ. Here, $p_{\rm T,min}$ and $p_{\rm T,max}$ specify the transverse momentum range of the measurement. The quantities $\Delta p_{\rm T,i} = p_{\rm T,i} - \langle p_{\rm T}\rangle$, where $i = 1,2$, are deviations from the average transverse momentum calculated as follows

$$\langle p_{\rm T}\rangle = \int_{p_{\rm T,min}}^{p_{\rm T,max}} \rho_1 p_{\rm T} {\rm d}p_{\rm T} / \int_{\rm p_{T,min}}^{\rm p_{T,max}} \rho_1 {\rm d}p_{\rm T}. \tag{6}$$

By construction, both R_2 and P_2 are robust observables to first order. Their magnitude remains insensitive to particle losses (i.e., detection inefficiencies) provided that these inefficiencies exhibit only modest dependence on kinematic variables, assuming the efficiency is uniform across the $p_{\rm T}$ acceptance of the measurement. Furthermore, both observables are dimensionless and their magnitude can be used as reliable measure of the degree of correlation between the produced particles. However, P_2 explicitly incorporates deviations of particle momenta to the mean and is therefore sensitive to the “hardness" of the correlations. This means it can distinguish whether correlated particle pairs involve soft–soft or hard–hard interactions, i.e., both particles below $\langle p_{\rm T}\rangle$ or both above $\langle p_{\rm T}\rangle$. It can also identify soft–hard pairs, where one particle has a $p_{\rm T}$ below the mean and the other above. Additionally, it is important to note that the relative magnitudes of contributions from soft–soft, hard–hard, and soft–hard combinations may change as a function of the $(\Delta\eta,\Delta\varphi)$ pair separation. One expects, for instance, that particle correlations within jets should yield a preponderance of hard–hard correlations near the core (thrust axis) of a jet. However, soft–hard dominance is expected for pairs involving one particle near the thrust axis and one emitted at a large angle relative to that axis. This implies that P_2 features an added sensitivity to the angular ordering of particle production in jets as well as in resonance decays [29]. The scaling properties of R_2 and P_2 with system size have been described in Ref. [28].

In this work, the correlation functions R_2 and P_2 are reported as functions of $\Delta\eta$ and $\Delta\varphi$ by averaging their magnitude across the pair average pseudorapidity $\bar{\eta} \equiv \frac{1}{2}(\eta_1 + \eta_2)$ and average azimuthal angle $\bar{\varphi} \equiv \frac{1}{2}(\varphi_1 + \varphi_2)$ acceptance, according to

$$O(\Delta\eta,\Delta\varphi) = \frac{1}{\Omega(\Delta\eta)} \int_{\Omega} {\rm O}(\Delta\eta,\bar{\eta},\Delta\varphi,\bar{\varphi}){\rm d}\bar{\eta}{\rm d}\bar{\varphi}. \tag{7}$$

Here, $O(\Delta\eta,\Delta\varphi)$ is either $R_2(\Delta\eta,\Delta\varphi)$ or $P_2(\Delta\eta,\Delta\varphi)$. The variable $\Omega(\Delta\eta)$, which depends solely on the $\Delta\eta$, represents the width of the acceptance in $\bar{\eta}$ at a given value of $\Delta\eta$ and $\Delta\varphi$ [32]. Furthermore, R_2 and P_2 are determined for $\Delta\varphi$ modulo 2π and shifted by $-\pi/2$ for convenience of representation in the figures.

The measured densities ρ_1 and ρ_2 are directly impacted by detection inefficiencies. Given that these differ for positively and negatively charged particles at given values of η and φ, benefiting from the robustness of R_2 and P_2 correlation functions requires these to be measured independently for pairs of $(+,+)$, $(-,-)$, $(-+)$, and $(+,-)$ charged particles. Correlation functions for $(+-)$ and $(-+)$ pairs are then averaged to yield US correlation functions, $O^{{\rm US}} \equiv \frac{1}{2}[O^{+-} + O^{-+}]$, and correlation functions of pairs $(++)$ and $(--)$ are averaged to yield LS correlation functions, $O^{{\rm L}S} \equiv \frac{1}{2}[O^{--} + O^{++}]$. In turn, $O^{{\rm U}S}$ and $O^{{\rm L}S}$ correlation functions are combined into CI and CD correlation functions according to

$$O^{\rm CI} = \frac{1}{2}\left[O^{\rm US} + O^{\rm LS}\right], \tag{8}$$

$$O^{\rm CD} = \frac{1}{2}\left[O^{\rm US} - O^{\rm LS}\right]. \tag{9}$$

The CI functions measure the average of correlations between all charged particles, whereas the CD observables are sensitive to the difference of US and LS pairs and are thus largely driven by charge conservation effects.

The width σ_Ω of the near-side peak of R_2 and P_2 correlation functions of CI and CD pair combinations is calculated along the $\Delta\eta$ and $\Delta\varphi$ axes with the procedure already used in prior ALICE studies [21]

$$\sigma_\Omega = \left(\frac{\sum_i [O(\Omega_i) - T]\Omega_i^2}{\sum_i [O(\Omega_i) - T]} \right)^{1/2}, \tag{10}$$

where i iterates over the bins, and T is an offset or threshold value. Offsets are considered to prevent width values that are determined simply by the detector acceptance. In order to calculate the width along $\Delta\varphi$, offsets are estimated by averaging three narrow $\Delta\varphi$ intervals near the minimum of the $\Delta\varphi$ distribution. On the other hand, while evaluating the width along $\Delta\eta$, offsets are determined close to the edge of the acceptance, approximately at $\Delta\eta \approx 1.6$. Since the correlation vanishes for large $|\Delta\eta|$ values in the case of R_2^{CD}, a null offset is used, which results in the exclusion of contributions from the unobserved part beyond the acceptance [21].

The balance function (B) [33] of charged particles is also measured in minimum bias pp collisions. It is computed according to

$$B(\Delta\eta,\Delta\varphi) \equiv \left\langle \frac{\mathrm{d}^2 N_{\mathrm{ch}}}{\mathrm{d}\eta d\varphi} \right\rangle \times R_2^{\mathrm{CD}}(\Delta\eta,\Delta\varphi), \tag{11}$$

which applies when densities (yields) of positively and negatively charged particles are approximately equal [34, 35]. In addition, the integral of the charge balance function, I_{B}, is calculated according to

$$I_{\mathrm{B}} = \int_{\mathrm{d}\eta_{\min}}^{\mathrm{d}\eta_{\max}} \int_{\mathrm{d}\varphi_{\min}}^{\mathrm{d}\varphi_{\max}} \int_{\mathrm{d}p_{\mathrm{T,min}}}^{\mathrm{d}p_{\mathrm{T,max}}} B(\Delta\eta,\Delta\varphi)\mathrm{d}\eta\mathrm{d}\varphi\mathrm{d}p_{\mathrm{T}}. \tag{12}$$

The integral of B in pp collisions is compared with previously published results in Pb–Pb collisions [36]. This comparative study provides insights into how the charges are balanced and produced in both pp and Pb–Pb collisions.

3 Datasets and experimental method

Results reported in this work are based on an analysis of 4.4×10^8 minimum bias (MB) pp collisions at $\sqrt{s}$ = 13 TeV collected by the ALICE detector during the Run 2 data taking campaign in 2018. The MB trigger selects collisions with at least one hit in both the V0A and V0C detectors, which are scintillator arrays covering the pseudorapidity ranges $2.8 < \eta < 5.1$ and $-3.7 < \eta < -1.7$, respectively. Moreover, to minimize instrumental effects and maintain approximately uniform acceptance and efficiency as a function of pseudorapidity, only events having a reconstructed primary vertex (PV) within ±8 cm from the nominal center of the ALICE detector along the beam direction are considered in the analysis. Pile-up events involving multiple reconstructed vertices are rejected using offline algorithms [37]. Charged particle tracks included in this analysis were reconstructed using the Inner Tracking System (ITS) and the Time Projection Chamber (TPC) detectors. The design and performance of the V0, ITS, and TPC detectors are reported in Refs. [38–40].

The analysis is limited to charged-particle tracks reconstructed within the pseudorapidity range $|\eta| < 0.8$ and the transverse momentum interval $0.2 < p_{\mathrm{T}} < 2.0$ GeV/c to emphasize particle production governed by non-perturbative soft quantum chromodynamics (QCD) processes. The analysis includes selection criteria to suppress secondary charged particles (i.e., particles originating from weak decays, γ-conversions, and secondary hadronic interactions in the detector material) and fake tracks (random associations of space points). The used track parameters are obtained by the Kalman filter at the collision primary vertex. Tracks of particles originating from weak decays of $\mathrm{K}^0_{\mathrm{S}}$ and Λ^0 and other secondaries are suppressed based on a p_{T}-dependent selection on the distance of closest approach (DCA) of charged particle trajectories to the PV [41]. Electrons and positrons are rejected based on their specific energy loss (dE/dx) measured within the TPC. Good track quality is assured by retaining only tracks with more than 70 reconstructed TPC space points, out of a maximum of 159 and a momentum fit with a χ^2-value per degree of freedom less than 2.0. In order to increase the track quality and further suppress tracks produced in pile-up of collisions occurring within the long TPC readout time, the selected tracks are required to have a combined refit in both the ITS and the TPC and at least one hit in the innermost part of the ITS.

Equations 1– 7 are used to obtain the R_2 and P_2 correlation functions as discussed in the previous section. Given that the accuracy of R_2 and P_2 may be impacted by $p_{\rm T}$-dependent inefficiencies, both R_2 and P_2 correlation functions are explicitly corrected for such dependencies [28]. The efficiencies are determined using Monte Carlo simulations of pp collisions based on the PYTHIA8 [42] event generator and the GEANT4 [43] transport code, as explained in detail in Sec. 4.

4 Monte Carlo model studies

Monte Carlo (MC) simulations of pp collisions at $\sqrt{s} = 13$ TeV generated with PYTHIA8 [42] are used to determine efficiency correction factors, evaluate the performance of the analysis procedure (also known as closure test), and produce the correlation functions compared with the experimental data in Sec. 6. The PYTHIA8 event generator is based on a QCD description of quark and gluon interactions at the leading order (LO) and uses the Lund string fragmentation model [44] for high-$p_{\rm T}$ parton hadronization. The production of soft particles (i.e., the underlying event) is handled through fragmentation of mini-jets from initial and final state radiation, as well as multiple parton interactions [45]. The calculations are performed with the Monash 2013 tune of PYTHIA8 running in minimum-bias mode, with soft QCD processes and color reconnection turned on [42].

Single particle detection efficiencies are estimated based on the ratio of detector and generator levels single particle yields obtained with PYTHIA8. Reconstructed (REC) level yields are obtained by propagating PYTHIA8 events through a model of the ALICE detector with GEANT4 and reconstructing the simulated events with the same software used for real data. Generator (GEN) level yields are obtained directly from the primary particles produced by PYTHIA8, without including efficiency losses or resolution smearing. Subsequently, tracking efficiency corrections are applied to both single- and two- particle pairs; these corrections cancel to first order in the calculations of R_2 and P_2.

A MC closure test is also carried out based on simulated PYTHIA8 events processed with GEANT4 and the full ALICE reconstruction of R_2 and P_2 correlation functions. The REC calculations are compared with correlation functions obtained at the GEN level to identify possible biases in the experimental determination of these measurements. Differences between reconstructed and generator level R_2 and P_2 correlation functions are found to be of the order or smaller than 1%. These differences, though modest, are conservatively added in the evaluation of systematic uncertainties discussed in the next section.

Furthermore, small particle losses are caused by momentum resolution near the edges of the acceptance: when charged particles from the generator level pass through GEANT4, a slight shift in η and $p_{\rm T}$ due to resolution effects could move these particles outside of the acceptance, leading to particle loss. This was addressed by excluding particles from the MC model that fell outside the acceptance and comparing the results with those obtained using the default approach, in which those particles were retained. The resulting difference was assigned as a part of the systematic uncertainty.

5 Determination of statistical and systematic uncertainties

Given the fact that the statistical uncertainties of the correlation functions are highly correlated, the final statistical uncertainties are estimated with the sub-sample method [46]. Overall, eleven data samples,

Table 1: Sources of systematic uncertainties.

Parameter	Default	Variation
$\mathrm{DCA}_{\mathrm{xy,z}}$(cm)	0.2	0.1
Track selection	Global tracks	tracks reconstructed based only on TPC information
Tracking efficiency	With	Without
Magnetic field polarity (T)	+0.5	-0.5
No. of TPC space points	>70	>90
Particle loss	With	Without
Track pile-up	Removed	Included
Event pile-up	Removed	Included

Table 2: Maximum systematic uncertainties of the correlation functions and their sources for projections.

Correlator	Category	Source	Maximum systematic uncertainties (%)
R_2^{CI}	$\Delta\eta$	Tracking efficiency	0.19
	$\Delta\varphi$	Tracking efficiency	0.13
P_2^{CI}	$\Delta\eta$	MC closure test	0.04
	$\Delta\varphi$	MC closure test	0.03
R_2^{CD}	$\Delta\eta$	MC closure test	0.04
	$\Delta\varphi$	MC closure test	0.03
P_2^{CD}	$\Delta\eta$	$\mathrm{DCA}_{\mathrm{xy,z}}$	0.0008
	$\Delta\varphi$	No. of TPC spcae points	0.0013

obtained by splitting the full data sample collected during the 2018 period, are used in the analysis separately. Their weighted mean constitutes the final result and the standard deviations from the mean are used to estimate the statistical uncertainties on the amplitude of the correlation functions.

Systematic uncertainties are estimated by repeating the analysis with modified event and charged-track selection criteria for LS, US, CI, and CD pairs separately. The criteria are varied individually to assess their impact on the measured correlation functions and their characteristics. As discussed in Sec. 4, a correction for the tracking efficiency is applied in the default analysis procedure. To estimate the systematic uncertainty due to possible imperfections in the description of the tracking efficiency, the analysis was repeated without applying this correction. A similar approach is applied to estimate the systematic uncertainty due to the correction for particle loss. As a cross check that no bias is introduced by the pile-up rejection at the event and track selection levels, the analysis was repeated without pile-up removal and a negligible effect on the results was found. The different selection criteria used to estimate the systematic uncertainties are described below and listed in Tab. 1. The Barlow criterion [47] is used to assess the statistical significance of differences observed when changing the selection criteria relative to the nominal analysis. Total systematic uncertainties are estimated by assuming that the different sources are independent: contributions from the various sources are summed in quadrature to obtain the total systematic uncertainties on the amplitude of the R_2 and P_2 correlation functions, as well as quantities derived from these. The maximum contributions of systematic uncertainties and their sources are presented in Tab. 2 and 3 for the projections and widths of the correlation functions, respectively.

Tracking efficiency contributes the most to the systematic uncertainties for projections of R_2^{CI} along $\Delta\eta$ ($\Delta\varphi$), which is roughly 0.19% (0.13%). Similarly, the highest contribution to the systematic uncertainties of the projections of R_2^{CD} and P_2^{CI} is 0.04% (0.03%) along $\Delta\eta$ ($\Delta\varphi$), resulting from Monte Carlo closure tests. The largest contribution to the systematic uncertainties for projections of P_2^{CD} along $\Delta\eta$ ($\Delta\varphi$) is 0.0008% (0.0013%), which is due to DCA (impact of the TPC sector boundaries). Contributions to the systematic uncertainties from other sources are found to be negligible.

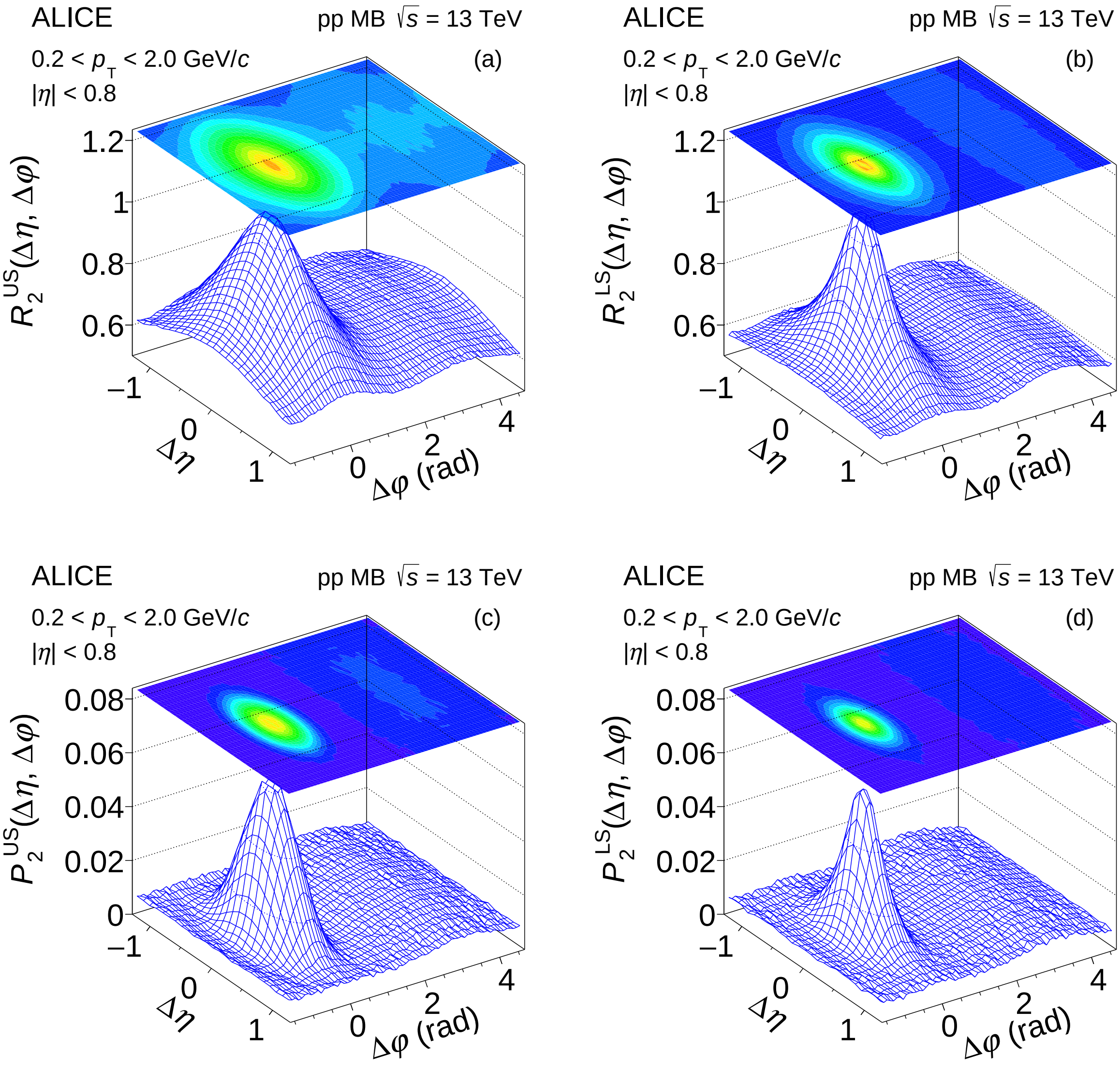

Figure 1: Correlation functions (a) R_2^{US}, (b) R_2^{LS}, (c) P_2^{US}, (d) P_2^{LS} of charged hadrons measured in minimum bias pp collisions at $\sqrt{s}$ = 13 TeV. Charged hadrons are selected in the range $0.2 < p_{\mathrm{T}} < 2.0$ GeV/c and with pseudorapidity $|\eta| < 0.8$.

The systematic uncertainties on the widths of the correlation functions, presented in Sec. 6.5, were assessed in a similar fashion by varying selection criteria individually. Contamination from secondaries not rejected by the DCA selection criteria contribute the most to these uncertainties, approximately 0.36% (0.59%), on the width of R_2^{CI} (P_2^{CI}) along $\Delta\eta$. The largest contribution to the systematic uncertainties in the width of R_2^{CI} (P_2^{CI}) as a function of $\Delta\varphi$ arises from track pile-up effects (tracking efficiency), amounting to approximately 0.58% (0.27%). However, the highest contribution to the systematic uncertainties on the width of R_2^{CD} along $\Delta\eta$ ($\Delta\varphi$) is 0.46% (2.17%) and originates from uncertainties on track reconstruction efficiencies. Tracking efficiencies (impact of the TPC sector boundaries) give rise the biggest contribution to the systematic uncertainties for the width of P_2^{CD} along $\Delta\eta$ ($\Delta\varphi$), which is around 0.54% (1.77%). Contributions from other sources are insignificant in this case.

The systematic uncertainties on the single particle density, shown in Sec. 6.6, contribute the most to the systematic uncertainties on the magnitude of the balance function and its integral. Altogether, the systematic uncertainty on the integral amounts to 5.8%, with the contribution due to single particle

Table 3: Maximum systematic uncertainties of the correlation functions and their sources for widths.

Correlator	Category	Source	Maximum systematic uncertainties (%)
$R_2^{\rm CI}$	$\Delta\eta$	$\rm DCA_{xy,z}$	0.36
	$\Delta\varphi$	Track pile-up	0.58
$P_2^{\rm CI}$	$\Delta\eta$	$\rm DCA_{xy,z}$	0.59
	$\Delta\varphi$	Tracking efficiency	0.27
$R_2^{\rm CD}$	$\Delta\eta$	Tracking efficiency	0.46
	$\Delta\varphi$	Tracking efficiency	2.17
$P_2^{\rm CD}$	$\Delta\eta$	Tracking efficiency	0.54
	$\Delta\varphi$	No. of TPC spcae points	1.77

density accounting for about 5.7%.

6 Results

The R_2 and P_2 correlation functions were first determined in two dimensions, i.e., as functions of particle pair pseudorapidity difference ($\Delta\eta$) and azimuthal angle difference ($\Delta\varphi$). These were then projected onto $\Delta\eta$ and $\Delta\varphi$ axes to further examine the dependence of the correlation functions on these kinematic variables.

6.1 Charge combinations of correlation functions

The R_2 and P_2 correlation functions for US and LS charged-particle pairs forming the basis of the measurements are displayed in Fig. 1. These correlation functions share common features, but also exhibit significant differences. All four correlation functions are dominated by the presence of a strong and relatively narrow peak centered at $(\Delta\eta,\Delta\varphi) = (0,0)$, hereafter called the near-side peak because it corresponds to the emission of two particles near one another in $\Delta\varphi$. The correlation functions also feature extended structures, of a smaller amplitude, hereafter called away-side, because they correspond to particle emission in two different hemispheres, at $\Delta\varphi \approx 180^\circ$. However, it is important to note also that US correlation functions feature a wider peak on the near-side as shown in Figs. 1 (a) and (c), whereas the LS ones exhibit a relatively narrower near-side peak, as shown in Figs. 1 (b) and (d). The narrower shape of the near-side peak of the LS correlation functions arises, in part, from Bose–Einstein quantum statistics (also known as Hanbury Brown–Twiss (HBT) effect): two identical mesons (e.g., $\pi^+\pi^+$) are likely to be emitted in nearly the same direction with similar transverse momenta. The longitudinal and azimuthal widths of the LS near-side peak shall thus be partially driven by the inverse of the system size (in spatial coordinates) [48]. Moreover, it can be observed that away-side structures have slightly different shapes and dependence on $\Delta\eta$. These near- and away-side shapes have formerly been observed in measurements of C_2 correlation functions (involving a particle with higher $p_{\rm T}$, known as trigger particle and a second particle considered as associate) measured in several collision systems and a variety of beam energies [21, 24, 49–52]. Several different mechanisms, including dijet, resonance decays, Bose–Einstein correlations, collective flow, and conservation of energy and momentum, are thought to be responsible for the near- and away-side shapes [53–55]. Furthermore, it can be observed that the US and LS combinations of P_2 correlation functions exhibit similar behaviors, but significantly narrower near-side peaks as compared to R_2, as seen in Figs. 1 (c) and (d). The R_2 and P_2 US and LS correlation functions, shown in Fig. 1, are combined using Eqs. 8 and 9, respectively. This combination produces the CI and CD of R_2 and P_2 correlation functions presented in Figs. 2 and 4.

6.2 Charge-Independent (CI) correlation functions

The R_2 and P_2 correlation functions for CI combinations, shown in the left and right panels of Fig. 2, are obtained by averaging US and LS correlation functions. Hence, they evidently feature rather similar

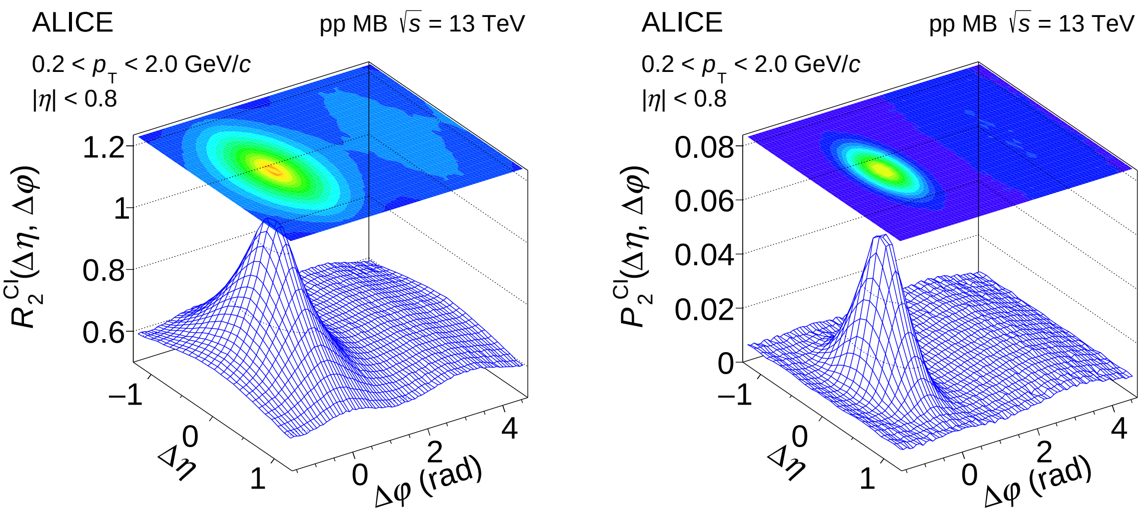

Figure 2: Correlation functions $R_2^{\rm CI}$ (left) and $P_2^{\rm CI}$ (right) of charged hadrons measured in minimum bias pp collisions at $\sqrt{s} = 13$ TeV. Charged hadrons are selected in the range $0.2 < p_{\rm T} < 2.0$ GeV/c and with pseudorapidity $|\eta| < 0.8$.

dependencies on $\Delta\eta$ and $\Delta\varphi$. Indeed, both correlation functions have a strong near-side peak centered at $(\Delta\eta,\Delta\varphi) = (0,0)$ and an away-side structure centered at $\Delta\varphi = \pi$ and extending over the whole $|\Delta\eta|$ range. It can be seen, however, that the near-side peak of $P_2^{\rm CI}$ is significantly narrower than the near-side peak of $R_2^{\rm CI}$. This is better visible in Fig. 3 which presents the projections of $R_2^{\rm CI}$ and $P_2^{\rm CI}$ onto $\Delta\eta$ and $\Delta\varphi$ axes in the left and right panels, respectively. It is clear that the near-side peak of the $P_2^{\rm CI}(\Delta\eta)$ correlation function is narrower than the corresponding peak of $R_2^{\rm CI}(\Delta\eta)$. It is worth stressing, however, that R_2 and P_2 correlation functions have the same kernel, i.e., the same source of correlated particles. The fact that the $P_2^{\rm CI}$ near-side peak is narrower relative to that of $R_2^{\rm CI}$ is thus associated with the $\Delta p_{\rm T}\Delta p_{\rm T}$ dependence of the former: at some large relative angles and pseudorapidity differences, the factor $\Delta p_{\rm T}\Delta p_{\rm T}$ manifestly suppresses the amplitude of the P_2 correlation function. In the tail of the near-side peak, the contributions of particle pairs with positive and negative values of $\Delta p_{\rm T}\Delta p_{\rm T}$ are similar between each other and thereby essentially cancel one another leading to a suppression of the apparent strength of particle correlations in that range. At small values of $\Delta\eta$ and $\Delta\varphi$, pairs with $\Delta p_{\rm T}\Delta p_{\rm T} > 0$ clearly dominate and yield the narrow peak observed. This behavior is consistent with the angular ordering expected in jets as confirmed by model calculations based on PYTHIA8 [29]. The effect is, however, also expected from hadronic resonance decays. It should be additionally noted that a similar pattern was observed for $R_2^{\rm CI}$ and $P_2^{\rm CI}$ correlation functions measured in p–Pb and Pb–Pb collisions [21].

6.3 Charge-Dependent (CD) correlation functions

The $R_2^{\rm CD}$ and $P_2^{\rm CD}$ correlation functions are shown as two-dimensional plots in the left and right panels of Fig. 4, respectively, and their projections onto $\Delta\eta$ and $\Delta\varphi$ axes are displayed in Fig. 5. It can be noted that the near-side peak of both correlation functions feature a narrow dip around $(\Delta\eta,\Delta\varphi) = (0,0)$, which stems in large part due to Bose–Einstein Quantum Statistics. In addition, the near-side peak of the $P_2^{\rm CD}$ correlation function is substantially narrower than that of $R_2^{\rm CD}$. This difference is expected from the angular and transverse momentum ordering effect already mentioned [29].

At LHC energies, positively and negatively charged particles are produced in nearly equal multiplicities and feature similar $p_{\rm T}$ spectra [56]. In large collision systems, negatively and positively charged particles are found to have nearly equal momentum anisotropy distributions. It entails that in large systems, the $R_2^{\rm CD}$ and $P_2^{\rm CD}$ correlation functions feature an essentially flat and featureless away-side across a wide interval of collision centrality spanning from the most central collisions down to peripheral collisions.

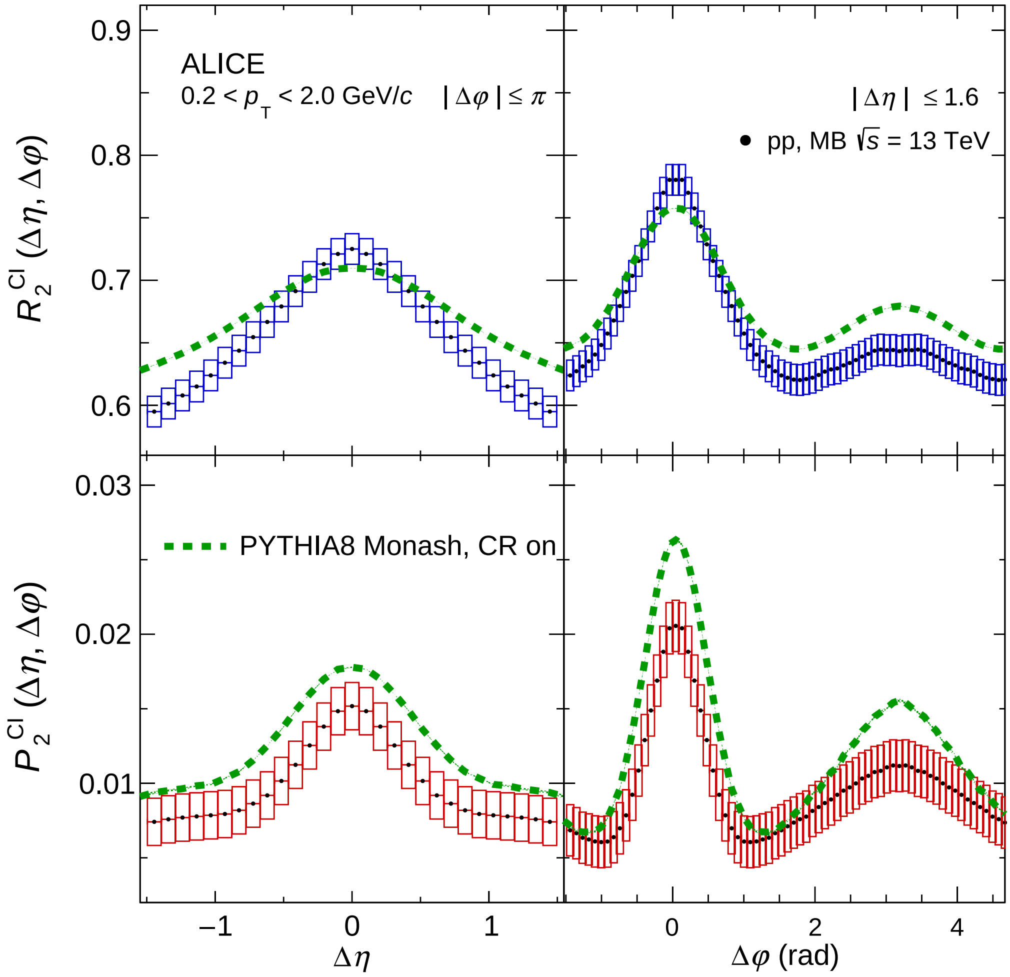

Figure 3: Projections onto $\Delta\eta$ (left column) and $\Delta\varphi$ (right column) of R_2^{CI} (top row) and P_2^{CI} (bottom row) correlation functions of charged hadrons calculated in the selected p_T range in pp collisions at $\sqrt{s} = 13$ TeV. The $\Delta\eta$ and $\Delta\varphi$ projections are calculated as averages of the two-dimensional correlations in the range $|\Delta\varphi| \le \pi$ and $|\Delta\eta| \le 1.6$, respectively. Vertical bars and boxes represent statistical and systematic uncertainties, respectively. Simulations using PYTHIA8 with the Monash 2013 tune and color reconnection (CR) enabled, as described in the text, are shown as green dashed lines.

While particle momentum anisotropies, possibly originating from a collectively expanding system, have been observed in high-multiplicity pp collisions, it is expected that non-flow correlations, such as those resulting from energy–momentum conservation (causing back-to-back particle emission in the transverse plane), should impact LS and US charged particle pairs similarly and thus lead to a flat away-side distribution. It can be observed, however, that the away-side of the R_2^{CD} correlation function is not flat and shows a dependence on both $\Delta\eta$ and $\Delta\varphi$ which reflects a small difference in the away-side emission of LS and US pairs. This likely results from the rather broad nature of the near-side peak, which extends beyond $\Delta\varphi = \pi/2$ towards the away-side. In contrast, however, the P_2^{CD} near-side peak is narrower and does not extend on the away-side. This correlation function thus has a rather flat away-side. This behavior was also observed in p–Pb and Pb–Pb collisions [21].

6.4 R_2 and P_2 correlation functions with PYTHIA8

The PYTHIA8 [42] event generator has had great successes in modeling recent measurements of single particle and jet production in high-energy pp collisions. It is thus of interest to investigate whether it can

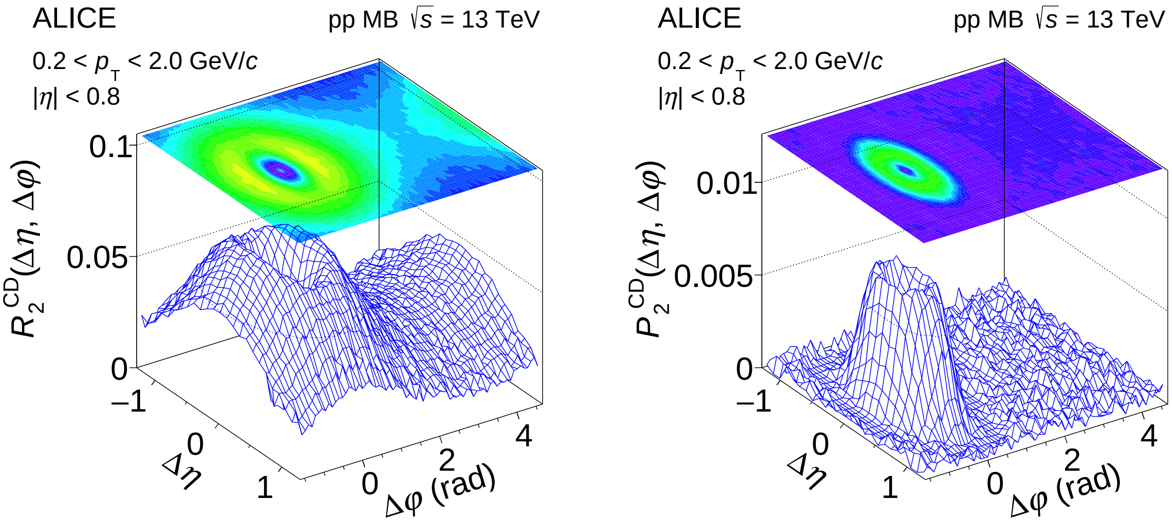

Figure 4: Correlation functions R_2^{CD} (left) and P_2^{CD} (right) of charged hadrons in minimum bias pp collisions at $\sqrt{s}$ = 13 TeV. Charged hadrons are selected in the range $0.2 < p_T < 2.0$ GeV/c and with pseudorapidity $|\eta| < 0.8$.

also reproduce the measured R_2 and P_2 correlation functions. Comparisons with PYTHIA8 calculations of CI and CD components of these correlation functions are presented in Figs. 3 and 5, respectively. Focusing on the $\Delta\eta$ (left) and $\Delta\varphi$ (right) projections of CI correlation functions, shown in Fig. 3, it can be noted that PYTHIA8 essentially captures the basic features of the R_2^{CI} and P_2^{CI} correlation functions. The projections indeed show near-side peaks and away-side structures that approximately match those observed experimentally. The small differences between the calculations and the measurements may originate from various phenomena, the detailed analysis of which is beyond the scope of this work.

Switching the discussion to the projections of the CD correlations, shown in Fig. 5, it can be observed that also in this case, PYTHIA8 captures the salient features of the measured correlation functions, with one notable exception: the dip structures found at $\Delta\eta = 0$ and $\Delta\varphi = 0$ in experimental data. By construction, CD correlations are sensitive to the presence of HBT, manifested in LS, and known to exist in all colliding systems. The HBT correlations, typically measured in terms of invariant momentum differences, are expected to be relevant at small $\Delta\eta$, $\Delta\varphi$ separation [57]. As such the width of the dip in the CD correlations reflects in part the width of the peak in LS correlations due to Bose–Einstein condensation and thus serve as an indicator of the system size. Such effects are not seen in the PYTHIA8 predictions shown in the figures because no HBT afterburner was used in the calculations [58]. It is also possible that the dip observed at small pair separation may arise from other causes related to particle production from hadronic resonance decays or other sources of charge conserving production mechanisms. Furthermore, PYTHIA8 also predicts the presence of a small bump structure centered at $\Delta\varphi = \pi$ in $\Delta\varphi$ projections of R_2^{CD} which is not observed in the data. Such small away-side peak is likely caused by momentum conservation effects which manifest themselves by back-to-back particle emission at low multiplicity. Similarly, PYTHIA8 reproduces the $P_2^{CD}(\Delta\eta)$ with some deviations near $\Delta\eta = 0$ and towards the edge. Moreover, it can be observed that in contrast to the R_2^{CD}, where PYTHIA8 approximately matches the overall magnitude of the correlation function, the near-side peak of the P_2^{CD} is overestimated by a factor of two while the away-side magnitude is underestimated by the same factor. These results show that while PYTHIA8 qualitatively reproduces the measured correlation functions, additional tuning of its parameters is required to fully match the data.

6.5 Evolution of the near-side peak width with multiplicity in different collision systems

The widths of the near-side peak of the measured correlation functions along the $\Delta\eta$ and $\Delta\varphi$ axes are commonly used to characterize the many processes that contribute to the strength and shape of particle

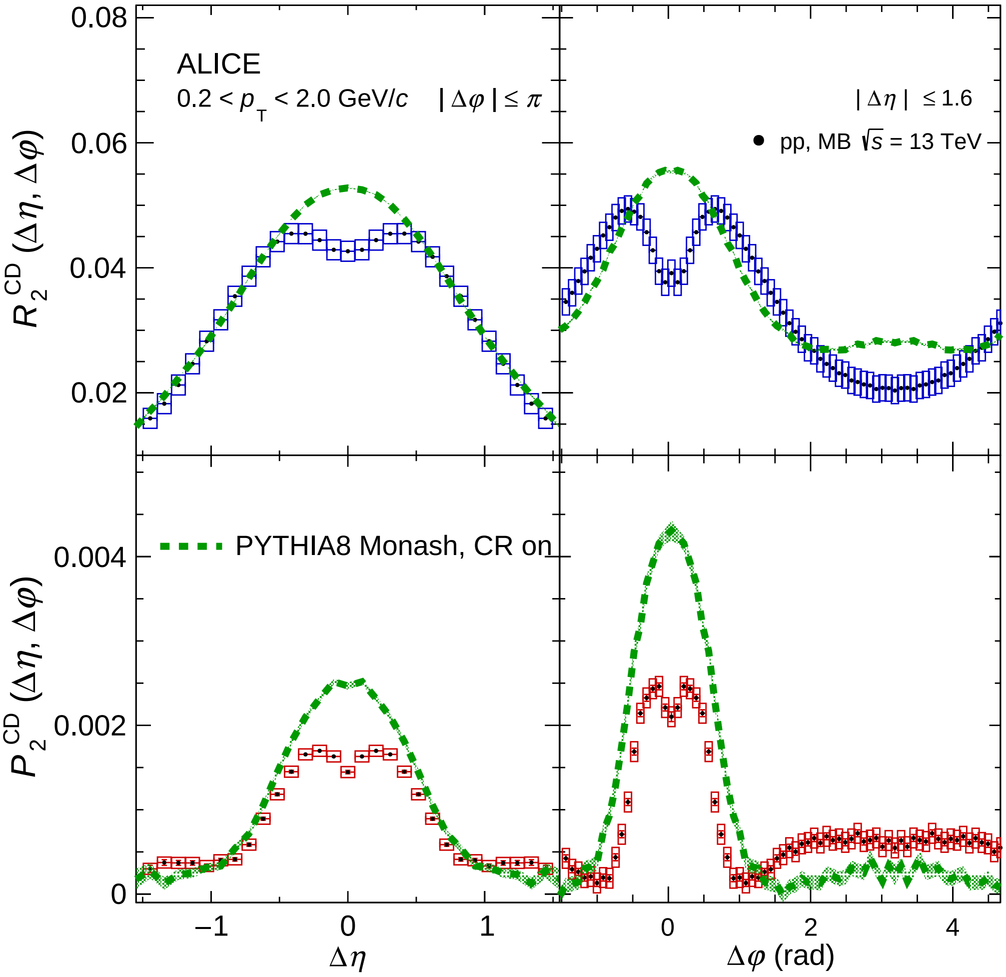

Figure 5: Projections onto the $\Delta\eta$ (left) and $\Delta\varphi$ (right) axes of the $R_2^{\rm CD}$ (top) and $P_2^{\rm CD}$ (bottom) correlation functions shown in Fig. 4. The $\Delta\eta$ and $\Delta\varphi$ projections are calculated as averages of the two-dimensional correlations in the range $|\Delta\varphi| \leq \pi$ and $|\Delta\eta| \leq 1.6$, respectively. Vertical bars and boxes represent statistical and systematic uncertainties, respectively. Simulations using PYTHIA8 with the Monash 2013 tune and color reconnection (CR) enabled, as described in the text, are shown as green dashed lines.

correlations. It is interesting, in particular, to consider how these widths evolve with the produced particle multiplicity quantified by the charged-particle pseudorapidity density at midrapidity ($\langle {\rm d}N_{\rm ch}/{\rm d}\eta\rangle_{|\eta|<0.5}$), the collision system size, as well as the collision energy.

This section reports the near-side peak root mean square (RMS) widths of correlation functions computed using Eq. (10) and shown in Figs. 6 and 7. Given some ambiguities existing in the identification of a baseline for broad peaks measured in a narrow acceptance, as in the case of the $\Delta\eta$ projections of $R_2^{\rm CI}$ and $P_2^{\rm CI}$, the RMS widths are computed using two methods: the first involves accounting for the presence of a baseline (or correlation plateau) underneath the peak and the second characterizes the width of the peak in a fixed $\Delta\eta$ or $\Delta\varphi$ range. In the case of the first method, since a plateau is not evident based on the shape of the projected correlation functions (reported in Fig. 3), the correlation strength at the edges of the acceptance is used as baseline and thus constitutes a somewhat arbitrary definition of the baseline, which ignores the correlation strength at $\Delta\eta$ values beyond the experimental acceptance. It nonetheless provides an estimator of the width of interest albeit with a bias. The second method has merits and limitations as well. It evidently does not suffer from the somewhat arbitrary requirement of a baseline

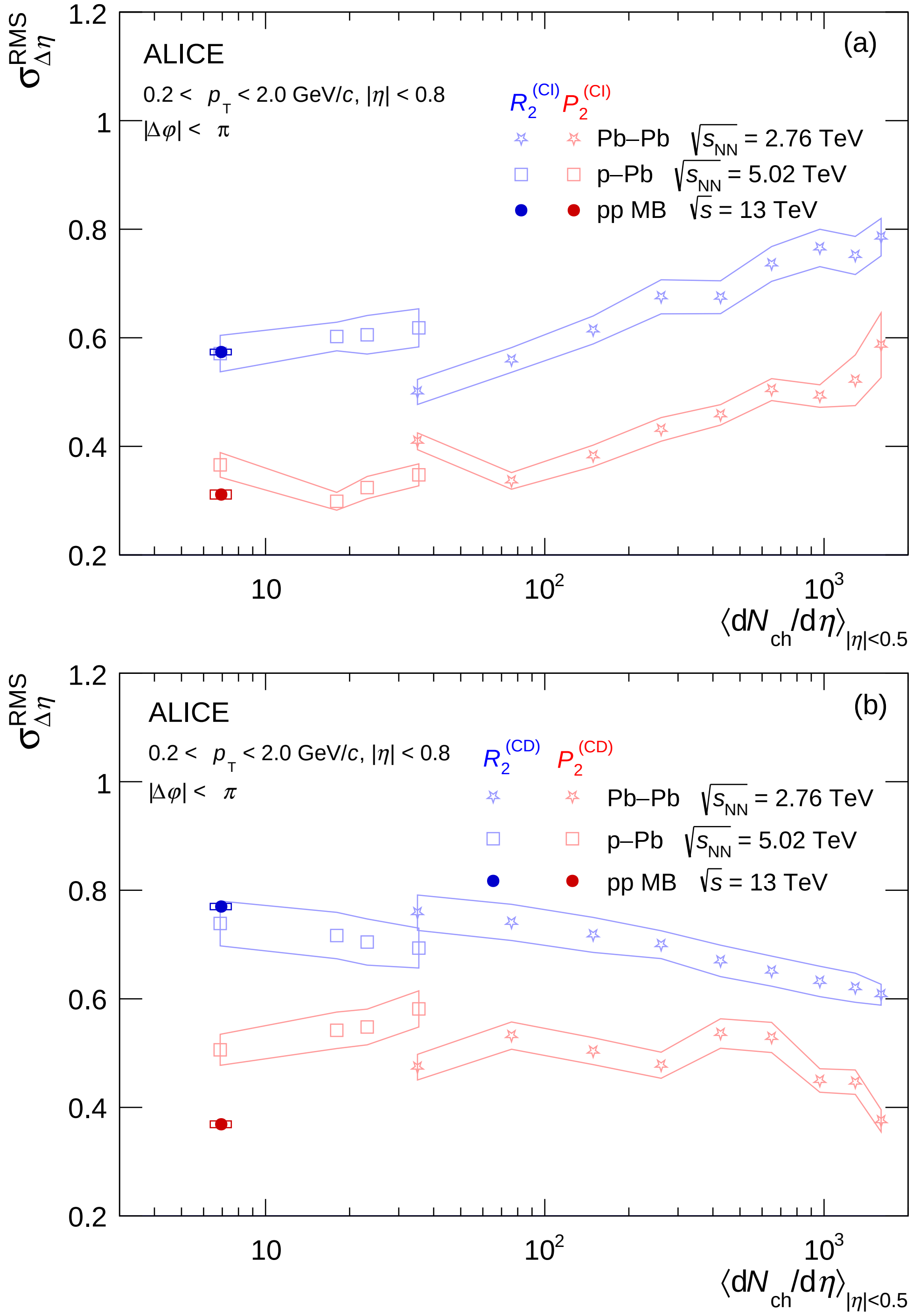

Figure 6: Width of (a) $R_2^{\rm CI}(\Delta\eta)$ (blue markers) and $P_2^{\rm CI}(\Delta\eta)$ (red markers) and (b) $R_2^{\rm CD}(\Delta\eta)$ (blue markers) and $P_2^{\rm CD}(\Delta\eta)$ (red markers) correlation functions along $\Delta\eta$ measured within $|\Delta\varphi| < \pi$ in pp collisions and compared with results from p–Pb and Pb–Pb collisions [21] as a function of $\langle {\rm d}N_{\rm ch}/{\rm d}\eta \rangle_{|\eta|<0.5}$. Vertical bars and boxes represent statistical and systematic uncertainties, respectively.

determination, but its magnitude is largely defined by the experimental acceptance itself. For instance, the offset for $P_2^{\rm CI}(\Delta\varphi)$, illustrated in Fig. 3, is determined by averaging three consecutive bins at the turning points near the edges of the near-side peak. Indeed, for a shallow peak or no peak whatsoever, the RMS width would be equal to the accepted range divided by $\sqrt{12}$.

The RMS widths of the R_2 and P_2 correlation functions computed with and without offsets (offset = 0) are

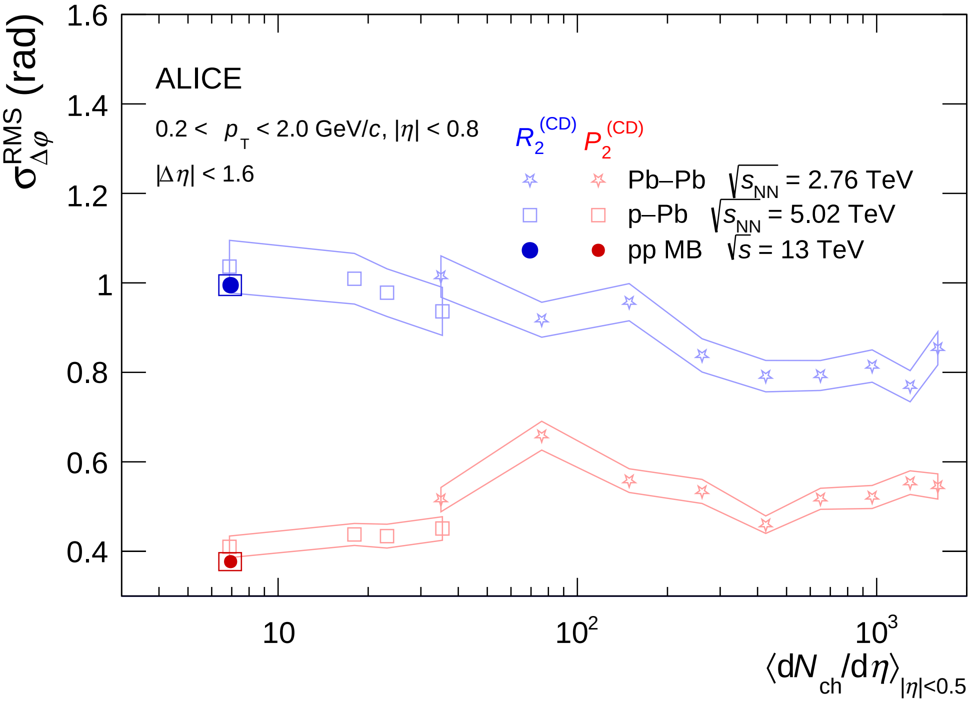

Figure 7: Widths of $R_2^{CD}(\Delta\varphi)$ (blue markers) and $P_2^{CD}(\Delta\varphi)$ (red markers) correlation functions along $\Delta\varphi$ measured within $|\Delta\eta| < 1.6$ for pp and within $|\Delta\eta| < 1.8$ for p–Pb and Pb–Pb collisions [21] as a function of $\langle dN_{ch}/d\eta\rangle_{|\eta|<0.5}$. Vertical bars and boxes represent statistical and systematic uncertainties, respectively.

Table 4: Comparison of the widths calculated with and without the offset (T = 0) in Eq. 10.

Correlator	Category	With Offset	Without Offset
R_2^{CI}	$\Delta\eta$	$0.57 \pm 0.0003(\text{stat.}) \pm 0.0052(\text{syst.})$	$0.90 \pm < 0.0001(\text{stat.}) \pm 0.0079(\text{syst.})$
	$\Delta\varphi$	$0.54 \pm 0.0002(\text{stat.}) \pm 0.0086(\text{syst.})$	$0.93 \pm < 0.0001(\text{stat.}) \pm 0.0148(\text{syst.})$
P_2^{CI}	$\Delta\eta$	$0.31 \pm 0.0007(\text{stat.}) \pm 0.041(\text{syst.})$	$0.51 \pm 0.0001(\text{stat.}) \pm 0.079(\text{syst.})$
	$\Delta\varphi$	$0.33 \pm 0.0007(\text{stat.}) \pm 0.004(\text{syst.})$	$0.51 \pm 0.0002(\text{stat.}) \pm 0.006(\text{syst.})$
R_2^{CD}	$\Delta\eta$	$0.65 \pm 0.001(\text{stat.}) \pm 0.0058(\text{syst.})$	$0.77 \pm 0.0004(\text{stat.}) \pm 0.0069(\text{syst.})$
	$\Delta\varphi$	$0.99 \pm 0.0025(\text{stat.}) \pm 0.023(\text{syst.})$	$1.27 \pm 0.001(\text{stat.}) \pm 0.0298(\text{syst.})$
P_2^{CD}	$\Delta\eta$	$0.37 \pm 0.0039(\text{stat.}) \pm 0.0062(\text{syst.})$	$0.51 \pm 0.0024(\text{stat.}) \pm 0.0084(\text{syst.})$
	$\Delta\varphi$	$0.37 \pm 0.0031(\text{stat.}) \pm 0.02(\text{syst.})$	$0.41 \pm 0.0025(\text{stat.}) \pm 0.0215(\text{syst.})$

reported in Tab. 4. Despite the fact that both methods mentioned above use an offset, the table enables a direct comparison between calculations performed with and without this offset. To maintain consistency with previous results in p–Pb and Pb–Pb, the widths for R_2^{CD} are considered without applying any offset. The computed RMS widths feature a strong dependence on the method chosen for their evaluation. Comparisons with the results of prior measurements and/or with model predictions must then be carried out in a consistent manner. Figures 6 and 7 compare the widths along $\Delta\eta$ and $\Delta\varphi$ obtained in pp collisions at $\sqrt{s}$ = 13 TeV, with those reported by the ALICE Collaboration in p–Pb collisions at $\sqrt{s_{NN}}$ = 5.02 TeV, and Pb–Pb collisions at $\sqrt{s_{NN}}$ = 2.76 TeV [21]. In the case of $R_2^{CD}(\Delta\eta)$, the RMS widths computed without offset are shown in Fig. 6, considering the fact that the correlation vanishes at large $|\Delta\eta|$ values, whereas finite offsets were used for other projections, consistent with the previous results in p–Pb and Pb–Pb collisions [21].

Figure 6 contrasts the longitudinal near-side widths of CI and CD correlation functions measured in pp collisions with those observed in p–Pb, and Pb–Pb collisions [21] as a function of the density of charged particles in the transverse momentum interval $0.15 < p_T < 20$ GeV/c and within the pseudorapidity range, $|\eta| < 0.5$ [59]. In the top panel of Fig. 6, it can be observed that the longitudinal RMS widths of $R_2^{\rm CI}(\Delta\eta)$ and $P_2^{\rm CI}(\Delta\eta)$ tend to rise with increasing particle density in p–Pb and Pb–Pb collisions, a feature that may be indicative of the finite shear viscosity of the medium created in these collisions, especially in Pb–Pb collisions [60, 61]. The longitudinal widths of $R_2^{\rm CD}$ measured in pp collisions are in a good agreement with those obtained in low multiplicity p–Pb collisions. In sharp contrast to that is a large deviation of the width of $P_2^{\rm CD}$ near-side peak from the value measured in p–Pb collisions with similar charged particle multiplicity. While the origin of this discrepancy is not entirely clear, it may in part arise from the difference in collision energy as well as mean-$p_{\rm T}$ [62] between pp and p–Pb collisions.

The evolution of the near-side peak width of $R_2^{\rm CD}(\Delta\varphi)$ correlation functions with produced particle multiplicity measured in pp, p–Pb, and Pb–Pb collisions is shown in Fig. 7. The observed decrease of the width from low to high multiplicity is likely due to the rise of the (transverse) radial flow in these collisions although it is also expected that the diffusivity of the matter produced in Pb–Pb collisions might induce a small broadening of the correlation function [30, 31]. The multiplicity dependence of the $P_2^{\rm CD}$ correlation function exhibits a more complicated behavior. The azimuthal width of $P_2^{\rm CD}$ displays a small rise from the multiplicity observed in minimum bias pp collisions to the largest multiplicities observed in p–Pb collisions. This rise continues up to $\langle {\rm d}N_{\rm ch}/{\rm d}\eta\rangle_{|\eta|<0.5} \approx 100$ in Pb–Pb, but is followed by a modest decrease at higher multiplicities. Again, it can be noted that the near-side peak of $P_2^{\rm CD}$ is considerably narrower than the one of $R_2^{\rm CD}$. Overall, it is visible that the azimuthal width of the $P_2^{\rm CD}$ near-side peak is smaller in pp and p–Pb than in Pb–Pb collisions. This suggests that the impact of the $p_{\rm T}$ angular ordering effect is weaker at high multiplicity perhaps owing to a greater probability of multiple scattering in such larger systems.

6.6 Balance function and its integral

Charge conservation dictates that the production of a positively charged particle must be accompanied by the creation of a charge balancing particle, i.e., a negatively charged particle. However, both production and transport mechanisms of charged particle pairs may impact the shape and strength of the $R_2^{\rm CD}$ correlation function. A focus on the particle production itself can be brought about by considering a measurement of charge balance function (B), which in the context of collisions at the LHC energies can be written: $B = \rho^{\rm B} R_2^{\rm CD}$, where $\rho^{\rm B}$ represents the charged particle density calculated in the kinematic range of $|\eta| < 0.8$ and $0.2 < p_{\rm T} < 2$ GeV/c. This single particle density is obtained by integration of prior ALICE measurements of the differential invariant yield of charged particles [59] according to

$$\rho^{\rm B} = \left\langle \frac{{\rm d}^2 N_{\rm ch}}{{\rm d}\varphi {\rm d}\eta} \right\rangle = \int_{p_{\rm T,min}}^{p_{\rm T,max}} \frac{{\rm d}^2 N_{\rm ch}}{2\pi p_{\rm T} {\rm d}p_{\rm T} {\rm d}\eta} \times p_{\rm T} {\rm d}p_{\rm T}. \tag{13}$$

The balance function as a function of $\Delta\eta$ and $\Delta\varphi$ is shown in the left panel of Fig. 8, and it has the same shape of the $R_2^{\rm CD}$ correlation function reported in Fig. 4(a) modulo a rescaling factor. The integral of the charge balance function, computed according to Eq. 12, amounts to $0.55 \pm 0.0039({\rm stat.}) \pm 0.06({\rm syst.})$ and it is shown in the right panel of Fig. 8. This means that given a positive hadron is measured in the acceptance $|\eta| < 0.8$, $0.2 < p_{\rm T} < 2.0$ GeV/c, the chance of finding a charge balancing negative hadron in that same particle acceptance amounts to 55%. The probability is evidently smaller than unity because the charge balancing hadron may be emitted (“leak") outside the acceptance, i.e., either at pseudorapidity $|\eta| > 0.8$ or outside the $0.2 < p_{\rm T} < 2.0$ GeV/c range of the measurement. It is worth noting, however, that this probability is compatible to the sum of the probabilities (in essentially identical acceptances) of observing π^-, $\rm K^-$, and $\overline{\rm p}$ as balancing partners of a π^+ in Pb–Pb collisions at $\sqrt{s_{\rm NN}} = 2.76$ TeV [36]. In this context, $\pi\pi$ pairs are predominantly observed, while contributions from other pairs are negligible. Nevertheless, the transverse momentum ranges for identified particles are different, and may account for the small modification. More detailed measurements of balance functions of identified hadrons in small and large collision systems and their evolution with produced particle multiplicity are forthcoming.

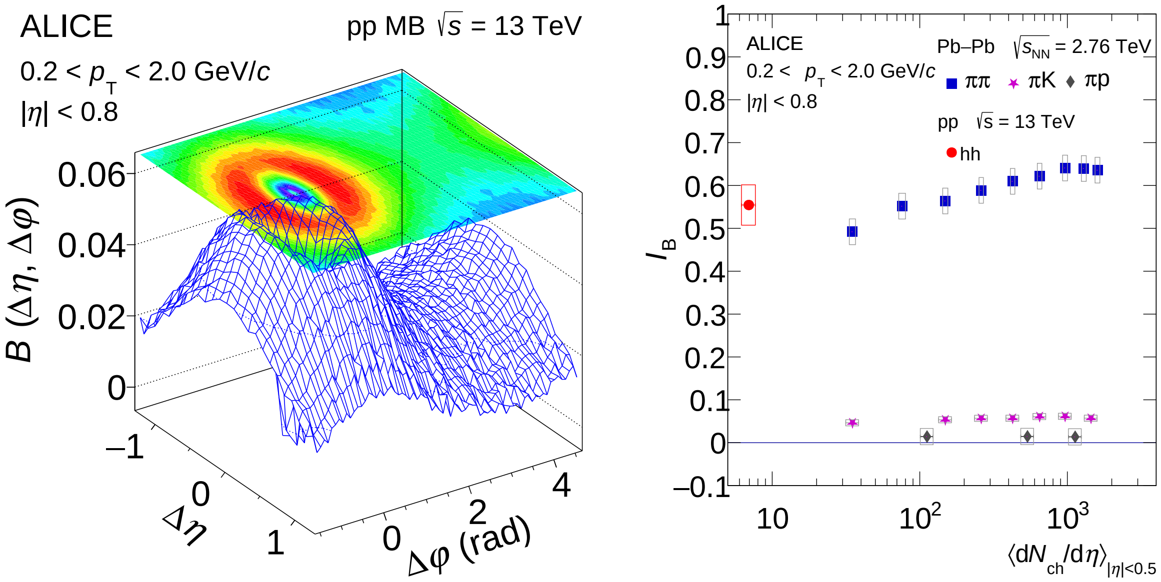

Figure 8: Balance function (left panel) of charged hadrons, in the selected p_T range, obtained using ALICE data in pp collisions at $\sqrt{s}$ = 13 TeV. Integral of B (right panel) results for charged hadrons in pp collisions at $\sqrt{s}$ = 13 TeV compared with the B integral of identified hadron ($\pi\pi$, πK, and πp) pairs in Pb–Pb collisions at $\sqrt{s_{NN}}$ = 2.76 TeV [36]. Vertical bars and boxes represent statistical and systematic uncertainties, respectively.

7 Summary

Two-particle differential number correlation function, $R_2(\Delta\eta,\Delta\varphi)$, and transverse momentum correlation function, $P_2(\Delta\eta,\Delta\varphi)$, of charged particles in the transverse momentum range $0.2 < p_T < 2.0$ GeV$/c$ and pseudorapidity range $|\eta| < 0.8$ are measured in minimum-bias pp collisions at a center-of-mass energy of $\sqrt{s}$ = 13 TeV. Correlation functions are studied individually for LS and US particle pairs and combined to obtain CI and CD. These correlation functions exhibit features similar to those observed in larger collision systems, including, in particular, a somewhat narrow, but prominent peak at small particle pair separation $\Delta\eta$, $\Delta\varphi$. As well as in prior measurements in p–Pb and Pb–Pb collisions, the near-side peak of both CI and CD P_2 correlations is found to be significantly narrower than those of R_2 correlations, a feature expected from momentum versus angular ordering in jets and hadronic resonance decays. The $R_2^{\rm CD}$ and $P_2^{\rm CD}$ exhibit a narrow dip at the center of their respective near-side peaks. This feature is understood to result in part from Bose–Einstein correlations of LS particles and the relatively small source size of pp collisions. The projections of measured $R_2(\Delta\eta,\Delta\varphi)$ and $P_2(\Delta\eta,\Delta\varphi)$ onto $\Delta\eta$ and $\Delta\varphi$ are compared with PYTHIA8 calculations. It is found that PYTHIA8 qualitatively reproduces measurements in pp collisions, but cannot catch all the observed features suggesting that further improvement of the model is needed.

The RMS widths of the near-side peak of $R_2^{\rm CI}$ along the longitudinal and $R_2^{\rm CD}$ along the longitudinal and azimuthal directions are found to be in good agreement with the widths of correlation functions observed at low charged particle multiplicity in p–Pb collisions. This agreement indicates the breadth of these correlation functions likely primarily depends on the produced multiplicity. However, the widths of $P_2^{\rm CI}$ and $P_2^{\rm CD}$ in the longitudinal direction observed in pp are significantly smaller than those measured in p–Pb collisions. The azimuthal width of $P_2^{\rm CD}$ observed in pp approximately matches the width measured in p–Pb at similar charged particle density. The widths of the near-side peaks of R_2 and P_2 correlation functions are studied in detail and compared with the measurements performed in larger colliding systems. The widths of the near-side peak of R_2 for CI and CD combinations follow a consistent trend despite of differences in the center-of-mass energy for the three systems. However, the widths of the near-side peak of $P_2(\Delta\eta)$ for CI and CD show some deviations in the three systems. These deviations may in part come from differences in collision energy [62].

Furthermore, the integral of the balance function ($I_{\rm B}$) is measured in pp collisions based on the $R_2^{\rm CD}$ correlation function. The magnitude of the integral is found to be compatible to the sum of balance function integrals measured for individual charged hadron pairs, $\pi\pi$, πK, and πp, in Pb–Pb collisions by the ALICE Collaboration. This suggests that balance functions and their integrals evolve rather slowly with system size and collision energy.

Acknowledgements

The ALICE Collaboration would like to thank all its engineers and technicians for their invaluable contributions to the construction of the experiment and the CERN accelerator teams for the outstanding performance of the LHC complex. The ALICE Collaboration gratefully acknowledges the resources and support provided by all Grid centres and the Worldwide LHC Computing Grid (WLCG) collaboration. The ALICE Collaboration acknowledges the following funding agencies for their support in building and running the ALICE detector: A. I. Alikhanyan National Science Laboratory (Yerevan Physics Institute) Foundation (ANSL), State Committee of Science and World Federation of Scientists (WFS), Armenia; Austrian Academy of Sciences, Austrian Science Fund (FWF): [M 2467-N36] and Nationalstiftung für Forschung, Technologie und Entwicklung, Austria; Ministry of Communications and High Technologies, National Nuclear Research Center, Azerbaijan; Conselho Nacional de Desenvolvimento Científico e Tecnológico (CNPq), Financiadora de Estudos e Projetos (Finep), Fundação de Amparo à Pesquisa do Estado de São Paulo (FAPESP) and Universidade Federal do Rio Grande do Sul (UFRGS), Brazil; Bulgarian Ministry of Education and Science, within the National Roadmap for Research Infrastructures 2020-2027 (object CERN), Bulgaria; Ministry of Education of China (MOEC) , Ministry of Science & Technology of China (MSTC) and National Natural Science Foundation of China (NSFC), China; Ministry of Science and Education and Croatian Science Foundation, Croatia; Centro de Aplicaciones Tecnológicas y Desarrollo Nuclear (CEADEN), Cubaenergía, Cuba; Ministry of Education, Youth and Sports of the Czech Republic, Czech Republic; The Danish Council for Independent Research | Natural Sciences, the VILLUM FONDEN and Danish National Research Foundation (DNRF), Denmark; Helsinki Institute of Physics (HIP), Finland; Commissariat à l'Energie Atomique (CEA) and Institut National de Physique Nucléaire et de Physique des Particules (IN2P3) and Centre National de la Recherche Scientifique (CNRS), France; Bundesministerium für Bildung und Forschung (BMBF) and GSI Helmholtzzentrum für Schwerionenforschung GmbH, Germany; General Secretariat for Research and Technology, Ministry of Education, Research and Religions, Greece; National Research, Development and Innovation Office, Hungary; Department of Atomic Energy Government of India (DAE), Department of Science and Technology, Government of India (DST), University Grants Commission, Government of India (UGC) and Council of Scientific and Industrial Research (CSIR), India; National Research and Innovation Agency - BRIN, Indonesia; Istituto Nazionale di Fisica Nucleare (INFN), Italy; Japanese Ministry of Education, Culture, Sports, Science and Technology (MEXT) and Japan Society for the Promotion of Science (JSPS) KAKENHI, Japan; Consejo Nacional de Ciencia (CONACYT) y Tecnología, through Fondo de Cooperación Internacional en Ciencia y Tecnología (FONCICYT) and Dirección General de Asuntos del Personal Academico (DGAPA), Mexico; Nederlandse Organisatie voor Wetenschappelijk Onderzoek (NWO), Netherlands; The Research Council of Norway, Norway; Pontificia Universidad Católica del Perú, Peru; Ministry of Science and Higher Education, National Science Centre and WUT ID-UB, Poland; Korea Institute of Science and Technology Information and National Research Foundation of Korea (NRF), Republic of Korea; Ministry of Education and Scientific Research, Institute of Atomic Physics, Ministry of Research and Innovation and Institute of Atomic Physics and Universitatea Nationala de Stiinta si Tehnologie Politehnica Bucuresti, Romania; Ministry of Education, Science, Research and Sport of the Slovak Republic, Slovakia; National Research Foundation of South Africa, South Africa; Swedish Research Council (VR) and Knut & Alice Wallenberg Foundation (KAW), Sweden; European Organization for Nuclear Research, Switzerland; Suranaree University of Technology (SUT), National Science and Technology Development Agency (NSTDA) and National Science, Research and Innovation Fund (NSRF via PMU-B B05F650021), Thailand; Turkish Energy, Nuclear and Mineral Research Agency (TENMAK), Turkey; National Academy of Sciences of Ukraine, Ukraine; Science and Technology Facilities Council (STFC), United Kingdom; National Science Foundation of the United States of America (NSF) and United States Department of Energy, Office of Nuclear Physics (DOE NP), United States of America. In addition, individual groups or members have received support from: Czech Science Foundation (grant no. 23-07499S), Czech Republic; FORTE project, reg. no. CZ.02.01.01/00/22_008/0004632, Czech Republic, co-funded by the European Union, Czech Republic; European Research Council (grant no. 950692), European Union; ICSC - Centro Nazionale di Ricerca in High Performance Computing, Big Data and Quantum Computing, European Union - NextGenerationEU; Academy of Finland (Center of Excellence in Quark Matter) (grant nos. 346327, 346328), Finland.

References

[1] **STAR** Collaboration, J. Adams *et al.*, “Experimental and theoretical challenges in the search for the quark gluon plasma: The STAR Collaboration’s critical assessment of the evidence from RHIC collisions”, *Nucl. Phys.* **A757** (2005) 102–183, `arXiv:nucl-ex/0501009 [nucl-ex]`.

[2] **PHENIX** Collaboration, K. Adcox *et al.*, “Formation of dense partonic matter in relativistic nucleus-nucleus collisions at RHIC: Experimental evaluation by the PHENIX Collaboration”, *Nucl. Phys.* **A757** (2005) 184–283, `arXiv:nucl-ex/0410003 [nucl-ex]`.

[3] **BRAHMS** Collaboration, I. Arsene *et al.*, “Quark gluon plasma and color glass condensate at RHIC? The perspective from the BRAHMS experiment”, *Nuclear Physics A* **757** (2005) 1–27.

[4] **PHOBOS** Collaboration, B. B. Back *et al.*, “The PHOBOS perspective on discoveries at RHIC”, *Nucl. Phys.* **A757** (2005) 28–101, `arXiv:nucl-ex/0410022 [nucl-ex]`.

[5] **ALICE** Collaboration, J. Adam *et al.*, “Measurement of jet suppression in central Pb–Pb collisions at $\sqrt{s_{\mathrm{NN}}}$ = 2.76 TeV”, *Phys. Lett. B* **746** (2015) 1–14, `arXiv:1502.01689 [nucl-ex]`.

[6] **ALICE** Collaboration, J. Adam *et al.*, “J/ψ suppression at forward rapidity in Pb–Pb collisions at $\sqrt{s_{\mathrm{NN}}}$ = 5.02 TeV”, *Phys. Lett. B* **766** (2017) 212–224, `arXiv:1606.08197 [nucl-ex]`.

[7] **CMS** Collaboration, A. M. Sirunyan *et al.*, “Measurement of prompt and nonprompt charmonium suppression in Pb–Pb collisions at 5.02 TeV”, *Eur. Phys. J. C* **78** (2018) 509, `arXiv:1712.08959 [nucl-ex]`.

[8] **CMS** Collaboration, A. M. Sirunyan *et al.*, “Measurement of nuclear modification factors of Υ(1S), Υ(2S), and Υ(3S) mesons in Pb–Pb collisions at $\sqrt{s_{\mathrm{NN}}}$ = 5.02 TeV”, *Phys. Lett. B* **790** (2019) 270–293, `arXiv:1805.09215 [hep-ex]`.

[9] **ALICE** Collaboration, S. Acharya *et al.*, “Production of charged pions, kaons, and (anti-)protons in Pb–Pb and inelastic pp collisions at $\sqrt{s_{\mathrm{NN}}}$ = 5.02 TeV”, *Phys. Rev. C* **101** (2020) 044907, `arXiv:1910.07678 [nucl-ex]`.

[10] **ALICE** Collaboration, S. Acharya *et al.*, “The ALICE experiment: a journey through QCD”, *Eur. Phys. J. C* **84** (2024) 813, `arXiv:2211.04384 [nucl-ex]`.

[11] **ALICE** Collaboration, K. Aamodt *et al.*, “Elliptic flow of charged particles in Pb–Pb collisions at 2.76 TeV”, *Phys. Rev. Lett.* **105** (2010) 252302, `arXiv:1011.3914 [nucl-ex]`.

[12] **ALICE** Collaboration, B. B. Abelev *et al.*, "Centrality, rapidity and transverse momentum dependence of J/ψ suppression in Pb–Pb collisions at $\sqrt{s_{\rm NN}}$=2.76 TeV", *Phys. Lett. B* **734** (2014) 314–327, `arXiv:1311.0214 [nucl-ex]`.

[13] H. Song, S. A. Bass, U. Heinz, T. Hirano, and C. Shen, "200 A GeV Au+Au collisions serve a nearly perfect quark-gluon liquid", *Phys. Rev. Lett.* **106** (2011) 192301, `arXiv:1011.2783 [nucl-th]`.

[14] Z. Qiu, C. Shen, and U. Heinz, "Hydrodynamic elliptic and triangular flow in Pb–Pb collisions at $\sqrt{s_{\rm NN}}$ = 2.76 TeV", *Phys. Lett. B* **707** (2012) 151–155, `arXiv:1110.3033 [nucl-th]`.

[15] H. Song, "Hydrodynamic Modeling and the QGP Shear Viscosity", *Eur. Phys. J. A* **48** (2012) 163, `arXiv:1207.2396 [nucl-th]`.

[16] C. Gale, S. Jeon, and B. Schenke, "Hydrodynamic Modeling of Heavy-Ion Collisions", *Int. J. Mod. Phys. A* **28** (2013) 1340011, `arXiv:1301.5893 [nucl-th]`.

[17] J. E. Bernhard, J. S. Moreland, and S. A. Bass, "Bayesian estimation of the specific shear and bulk viscosity of quark–gluon plasma", *Nature Phys.* **15** (2019) 1113–1117.

[18] **ALICE** Collaboration, S. Acharya *et al.*, "Investigations of Anisotropic Flow Using Multiparticle Azimuthal Correlations in pp, p–Pb, Xe–Xe, and Pb–Pb Collisions at the LHC", *Phys. Rev. Lett.* **123** (2019) 142301, `arXiv:1903.01790 [nucl-ex]`.

[19] **ALICE** Collaboration, B. B. Abelev *et al.*, "Multiparticle azimuthal correlations in p–Pb and Pb–Pb collisions at the CERN Large Hadron Collider", *Phys. Rev. C* **90** (2014) 054901, `arXiv:1406.2474 [nucl-ex]`.

[20] **ALICE** Collaboration, J. Adam *et al.*, "Centrality Dependence of the Charged-Particle Multiplicity Density at Midrapidity in Pb–Pb Collisions at $\sqrt{s_{\rm NN}}$ = 5.02 TeV", *Phys. Rev. Lett.* **116** (2016) 222302, `arXiv:1512.06104 [nucl-ex]`.

[21] **ALICE** Collaboration, S. Acharya *et al.*, "Two particle differential transverse momentum and number density correlations in p–Pb and Pb–Pb at the LHC", *Phys. Rev. C* **100** (2019) 044903, `arXiv:1805.04422 [nucl-ex]`.

[22] S. Basu, V. Gonzalez, J. Pan, A. Knospe, A. Marin, C. Markert, and C. Pruneau, "Differential two-particle number and momentum correlations with the AMPT, UrQMD, and EPOS models in Pb–Pb collisions at $\sqrt{s_{\rm NN}}$=2.76 TeV", *Phys. Rev. C* **104** (2021) 064902, `arXiv:2001.07167 [nucl-ex]`.

[23] **ALICE** Collaboration, J. Adam *et al.*, "Multiplicity and transverse momentum evolution of charge-dependent correlations in pp, p–Pb, and Pb–Pb collisions at the LHC", *Eur. Phys. J. C* **76** (2016) 86, `arXiv:1509.07255 [nucl-ex]`.

[24] **ALICE** Collaboration, J. Adam *et al.*, "Flow dominance and factorization of transverse momentum correlations in Pb–Pb collisions at the LHC", *Phys. Rev. Lett.* **118** (2017) 162302, `arXiv:1702.02665 [nucl-ex]`.

[25] S. Basu, S. Chatterjee, R. Chatterjee, T. K. Nayak, and B. K. Nandi, "Specific Heat of Matter Formed in Relativistic Nuclear Collisions", *Phys. Rev. C* **94** (2016) 044901, `arXiv:1601.05631 [nucl-ex]`.

[26] S. Basu, S. Thakur, T. K. Nayak, and C. A. Pruneau, "Multiplicity and pseudorapidity density distributions of charged particles produced in pp, pA and AA collisions at RHIC & LHC energies", *J. Phys. G* **48** (2020) 025103, `arXiv:2008.07802 [nucl-ex]`.

[27] **ALICE** Collaboration, B. Abelev *et al.*, "Centrality determination of Pb–Pb collisions at $\sqrt{s_{\mathrm{NN}}}$ = 2.76 TeV with ALICE", *Phys. Rev. C* **88** (2013) 044909, `arXiv:1301.4361 [nucl-ex]`.

[28] M. Sharma and C. Pruneau, "Methods for the Study of Transverse Momentum Differential Correlations", *Phys. Rev. C* **79** (2009) 024905, `arXiv:0810.0716 [nucl-ex]`.

[29] B. Sahoo, B. K. Nandi, P. Pujahari, S. Basu, and C. Pruneau, "Simulation studies of $R_2(\Delta\eta,\Delta\varphi)$ and $P_2(\Delta\eta,\Delta\varphi)$ correlation functions in pp collisions with the PYTHIA and HERWIG models", *Phys. Rev. C* **100** (2019) 024909, `arXiv:1810.09747 [nucl-ex]`.

[30] S. Pratt, W. P. McCormack, and C. Ratti, "Production of Charge in Heavy Ion Collisions", *Phys. Rev. C* **92** (2015) 064905, `arXiv:1508.07031 [nucl-th]`.

[31] S. Pratt and C. Plumberg, "Determining the Diffusivity for Light Quarks from Experiment", *Phys. Rev. C* **102** (2020) 044909, `arXiv:1904.11459 [nucl-th]`.

[32] C. A. Pruneau, *Data Analysis Techniques for Physical Scientists*. Cambridge University Press, 2017.

[33] S. A. Bass, P. Danielewicz, and S. Pratt, "Clocking hadronization in relativistic heavy ion collisions with balance functions", *Phys. Rev. Lett.* **85** (2000) 2689–2692, `arXiv:nucl-th/0005044`.

[34] C. Pruneau, S. Gavin, and S. Voloshin, "Methods for the study of particle production fluctuations", *Phys. Rev. C* **66** (2002) 044904, `arXiv:nucl-ex/0204011`.

[35] **ALICE** Collaboration, J. Adam *et al.*, "Measurement of pion, kaon and proton production in proton–proton collisions at $\sqrt{s} = 7$ TeV", *Eur. Phys. J. C* **75** (2015) 226, `arXiv:1504.00024 [nucl-ex]`.

[36] **ALICE** Collaboration, S. Acharya *et al.*, "General balance functions of identified charged hadron pairs of (π,K,p) in Pb–Pb collisions at $\sqrt{s_{\mathrm{NN}}}$= 2.76 TeV", *Phys. Lett. B* **833** (2022) 137338, `arXiv:2110.06566 [nucl-ex]`.

[37] **ALICE** Collaboration, B. B. Abelev *et al.*, "Performance of the ALICE Experiment at the CERN LHC", *Int. J. Mod. Phys. A* **29** (2014) 1430044, `arXiv:1402.4476 [nucl-ex]`.

[38] **ALICE** Collaboration, K. Aamodt *et al.*, "The ALICE experiment at the CERN LHC", *JINST* **3** (2008) S08002.

[39] **ALICE** Collaboration, E. Abbas *et al.*, "Performance of the ALICE VZERO system", *JINST* **8** (2013) P10016, `arXiv:1306.3130 [nucl-ex]`.

[40] J. Alme *et al.*, "The ALICE TPC, a large 3-dimensional tracking device with fast readout for ultra-high multiplicity events", *Nucl. Instrum. Meth. A* **622** (2010) 316–367, `arXiv:1001.1950 [physics.ins-det]`.

[41] **ALICE** Collaboration, J. Adam *et al.*, "Charged-particle multiplicities in proton–proton collisions at $\sqrt{s} = 0.9$ to 8 TeV", *Eur. Phys. J. C* **77** (2017) 33, `arXiv:1509.07541 [nucl-ex]`.

[42] P. Skands, S. Carrazza, and J. Rojo, "Tuning PYTHIA 8.1: the Monash 2013 Tune", *Eur. Phys. J. C* **74** (2014) 3024, `arXiv:1404.5630 [hep-ph]`.

[43] **GEANT4** Collaboration, S. Agostinelli *et al.*, "GEANT4–a simulation toolkit", *Nucl. Instrum. Meth. A* **506** (2003) 250–303.

[44] B. Andersson, G. Gustafson, G. Ingelman, and T. Sjostrand, "Parton Fragmentation and String Dynamics", *Phys. Rept.* **97** (1983) 31–145.

[45] T. Sjostrand, S. Mrenna, and P. Z. Skands, "A Brief Introduction to PYTHIA 8.1", *Comput. Phys. Commun.* **178** (2008) 852–867, `arXiv:0710.3820 [hep-ph]`.

[46] P. R. Bevington and D. K. Robinson, *Data reduction and error analysis for the physical sciences; 3rd ed.* McGraw-Hill, New York, NY, 2003.

[47] R. Barlow, "Systematic errors: facts and fictions", `arXiv:0207026 [hep-ex]`.

[48] **ALICE** Collaboration, S. Acharya *et al.*, "Common femtoscopic hadron-emission source in pp collisions at the LHC", `arXiv:2311.14527 [hep-ph]`.

[49] **PHENIX** Collaboration, A. Adare *et al.*, "Transverse momentum and centrality dependence of dihadron correlations in Au+Au collisions at $\sqrt{s_{\rm NN}}$ = 200 GeV: Jet-quenching and the response of partonic matter", *Phys. Rev. C* **77** (2008) 011901, `arXiv:0705.3238 [nucl-ex]`.

[50] **STAR** Collaboration, J. Adams *et al.*, "Delta phi Delta eta Correlations in Central Au+Au Collisions at $\sqrt{s_{\rm NN}} = 200$ GeV", *Phys. Rev. C* **75** (2007) 034901, `arXiv:nucl-ex/0607003`.

[51] **STAR** Collaboration, B. I. Abelev *et al.*, "Long range rapidity correlations and jet production in high energy nuclear collisions", *Phys. Rev. C* **80** (2009) 064912, `arXiv:0909.0191 [nucl-ex]`.

[52] **PHENIX** Collaboration, A. Adare *et al.*, "Dihadron azimuthal correlations in Au+Au collisions at $\sqrt{s_{\rm NN}}$= 200 GeV", *Phys. Rev. C* **78** (2008) 014901, `arXiv:0801.4545 [nucl-ex]`.

[53] **ATLAS** Collaboration, G. Aad *et al.*, "Observation of Long-Range Elliptic Azimuthal Anisotropies in $\sqrt{s}$ =13 and 2.76 TeV pp Collisions with the ATLAS Detector", *Phys. Rev. Lett.* **116** (2016) 172301, `arXiv:1509.04776 [hep-ex]`.

[54] **CMS** Collaboration, V. Khachatryan *et al.*, "Observation of Long-Range Near-Side Angular Correlations in Proton-Proton Collisions at the LHC", *JHEP* **09** (2010) 091, `arXiv:1009.4122 [hep-ex]`.

[55] **CMS** Collaboration, V. Khachatryan *et al.*, "Measurement of long-range near-side two-particle angular correlations in pp collisions at $\sqrt{s}$ =13 TeV", *Phys. Rev. Lett.* **116** (2016) 172302, `arXiv:1510.03068 [nucl-ex]`.

[56] **ALICE** Collaboration, B. Abelev *et al.*, "Pion, Kaon, and Proton Production in Central Pb–Pb Collisions at $\sqrt{s_{\rm NN}}$ = 2.76 TeV", *Phys. Rev. Lett.* **109** (2012) 252301, `arXiv:1208.1974 [hep-ex]`.

[57] **ALICE** Collaboration, J. Adam *et al.*, "Two-pion femtoscopy in p–Pb collisions at $\sqrt{s_{\rm NN}}$ = 5.02 TeV", *Phys. Rev. C* **91** (2015) 034906, `arXiv:1502.00559 [nucl-ex]`.

[58] S. Pratt and C. Plumberg, "Evolving Charge Correlations in a Hybrid Model with both Hydrodynamics and Hadronic Boltzmann Descriptions", *Phys. Rev. C* **99** (2019) 044916, `arXiv:1812.05649 [nucl-th]`.

[59] **ALICE** Collaboration, J. Adam *et al.*, "Pseudorapidity and transverse-momentum distributions of charged particles in proton–proton collisions at $\sqrt{s} =$ 13 TeV", *Phys. Lett. B* **753** (2016) 319–329, `arXiv:1509.08734 [nucl-ex]`.

[60] **ALICE** Collaboration, S. Acharya *et al.*, "Longitudinal and azimuthal evolution of two-particle transverse momentum correlations in Pb–Pb collisions at $\sqrt{s_{\rm NN}}$ = 2.76 TeV", *Phys. Lett. B* **804** (2020) 135375, `arXiv:1910.14393 [nucl-ex]`.

[61] V. Gonzalez, S. Basu, P. Ladron De Guevara, A. Marin, J. Pan, and C. A. Pruneau, "Extraction of the specific shear viscosity of quark-gluon plasma from two-particle transverse momentum correlations", *Eur. Phys. J. C* **81** (2021) 465, `arXiv:2012.10542 [nucl-ex]`.

[62] **ALICE** Collaboration, B. B. Abelev *et al.*, "Multiplicity dependence of the average transverse momentum in pp, p–Pb, and Pb–Pb collisions at the LHC", *Phys. Lett. B* **727** (2013) 371–380, `arXiv:1307.1094 [nucl-ex]`.

A The ALICE Collaboration

S. Acharya[126], A. Agarwal[134], G. Aglieri Rinella[32], L. Aglietta[24], M. Agnello[29], N. Agrawal[25], Z. Ahammed[134], S. Ahmad[15], S.U. Ahn[71], I. Ahuja[36], A. Akindinov[140], V. Akishina[38], M. Al-Turany[96], D. Aleksandrov[140], B. Alessandro[56], H.M. Alfanda[6], R. Alfaro Molina[67], B. Ali[15], A. Alici[25], N. Alizadehvandchali[115], A. Alkin[103], J. Alme[20], G. Alocco[24,52], T. Alt[64], A.R. Altamura[50], I. Altsybeev[94], J.R. Alvarado[44], C.O.R. Alvarez[44], M.N. Anaam[6], C. Andrei[45], N. Andreou[114], A. Andronic[125], E. Andronov[140], V. Anguelov[93], F. Antinori[54], P. Antonioli[51], N. Apadula[73], L. Aphecetche[102], H. Appelshäuser[64], C. Arata[72], S. Arcelli[25], R. Arnaldi[56], J.G.M.C.A. Arneiro[109], I.C. Arsene[19], M. Arslandok[137], A. Augustinus[32], R. Averbeck[96], D. Averyanov[140], M.D. Azmi[15], H. Baba[123], A. Badalà[53], J. Bae[103], Y. Bae[103], Y.W. Baek[40], X. Bai[119], R. Bailhache[64], Y. Bailung[48], R. Bala[90], A. Balbino[29], A. Baldisseri[129], B. Balis[2], Z. Banoo[90], V. Barbasova[36], F. Barile[31], L. Barioglio[56], M. Barlou[77], B. Barman[41], G.G. Barnaföldi[46], L.S. Barnby[114], E. Barreau[102], V. Barret[126], L. Barreto[109], C. Bartels[118], K. Barth[32], E. Bartsch[64], N. Bastid[126], S. Basu[74], G. Batigne[102], D. Battistini[94], B. Batyunya[141], D. Bauri[47], J.L. Bazo Alba[100], I.G. Bearden[82], C. Beattie[137], P. Becht[96], D. Behera[48], I. Belikov[128], A.D.C. Bell Hechavarria[125], F. Bellini[25], R. Bellwied[115], S. Belokurova[140], L.G.E. Beltran[108], Y.A.V. Beltran[44], G. Bencedi[46], A. Bensaoula[115], S. Beole[24], Y. Berdnikov[140], A. Berdnikova[93], L. Bergmann[93], M.G. Besoiu[63], L. Betev[32], P.P. Bhaduri[134], A. Bhasin[90], B. Bhattacharjee[41], L. Bianchi[24], J. Bielčík[34], J. Bielčíková[85], A.P. Bigot[128], A. Bilandzic[94], G. Biro[46], S. Biswas[4], N. Bize[102], J.T. Blair[107], D. Blau[140], M.B. Blidaru[96], N. Bluhme[38], C. Blume[64], F. Bock[86], T. Bodova[20], J. Bok[16], L. Boldizsár[46], M. Bombara[36], P.M. Bond[32], G. Bonomi[133,55], H. Borel[129], A. Borissov[140], A.G. Borquez Carcamo[93], E. Botta[24], Y.E.M. Bouziani[64], L. Bratrud[64], P. Braun-Munzinger[96], M. Bregant[109], M. Broz[34], G.E. Bruno[95,31], V.D. Buchakchiev[35], M.D. Buckland[84], D. Budnikov[140], H. Buesching[64], S. Bufalino[29], P. Buhler[101], N. Burmasov[140], Z. Buthelezi[68,122], A. Bylinkin[20], S.A. Bysiak[106], J.C. Cabanillas Noris[108], M.F.T. Cabrera[115], H. Caines[137], A. Caliva[28], E. Calvo Villar[100], J.M.M. Camacho[108], P. Camerini[23], F.D.M. Canedo[109], S.L. Cantway[137], M. Carabas[112], A.A. Carballo[32], F. Carnesecchi[32], R. Caron[127], L.A.D. Carvalho[109], J. Castillo Castellanos[129], M. Castoldi[32], F. Catalano[32], S. Cattaruzzi[23], R. Cerri[24], I. Chakaberia[73], P. Chakraborty[135], S. Chandra[134], S. Chapeland[32], M. Chartier[118], S. Chattopadhay[134], M. Chen[39], T. Cheng[6], C. Cheshkov[127], D. Chiappara[27], V. Chibante Barroso[32], D.D. Chinellato[101], E.S. Chizzali[II,94], J. Cho[58], S. Cho[58], P. Chochula[32], Z.A. Chochulska[135], D. Choudhury[41], S. Choudhury[98], P. Christakoglou[83], C.H. Christensen[82], P. Christiansen[74], T. Chujo[124], M. Ciacco[29], C. Cicalo[52], F. Cindolo[51], M.R. Ciupek[96], G. Clai[III,51], F. Colamaria[50], J.S. Colburn[99], D. Colella[31], A. Colelli[31], M. Colocci[25], M. Concas[32], G. Conesa Balbastre[72], Z. Conesa del Valle[130], G. Contin[23], J.G. Contreras[34], M.L. Coquet[102], P. Cortese[132,56], M.R. Cosentino[111], F. Costa[32], S. Costanza[21,55], C. Cot[130], P. Crochet[126], M.M. Czarnynoga[135], A. Dainese[54], G. Dange[38], M.C. Danisch[93], A. Danu[63], P. Das[32,79], S. Das[4], A.R. Dash[125], S. Dash[47], A. De Caro[28], G. de Cataldo[50], J. de Cuveland[38], A. De Falco[22], D. De Gruttola[28], N. De Marco[56], C. De Martin[23], S. De Pasquale[28], R. Deb[133], R. Del Grande[94], L. Dello Stritto[32], W. Deng[6], K.C. Devereaux[18], P. Dhankher[18], D. Di Bari[31], A. Di Mauro[32], B. Di Ruzza[131], B. Diab[129], R.A. Diaz[141,7], Y. Ding[6], J. Ditzel[64], R. Divià[32], Ø. Djuvsland[20], U. Dmitrieva[140], A. Dobrin[63], B. Dönigus[64], J.M. Dubinski[135], A. Dubla[96], P. Dupieux[126], N. Dzalaiova[13], T.M. Eder[125], R.J. Ehlers[73], F. Eisenhut[64], R. Ejima[91], D. Elia[50], B. Erazmus[102], F. Ercolessi[25], B. Espagnon[130], G. Eulisse[32], D. Evans[99], S. Evdokimov[140], L. Fabbietti[94], M. Faggin[23], J. Faivre[72], F. Fan[6], W. Fan[73], A. Fantoni[49], M. Fasel[86], G. Feofilov[140], A. Fernández Téllez[44], L. Ferrandi[109], M.B. Ferrer[32], A. Ferrero[129], C. Ferrero[IV,56], A. Ferretti[24], V.J.G. Feuillard[93], V. Filova[34], D. Finogeev[140], F.M. Fionda[52], E. Flatland[32], F. Flor[137,115], A.N. Flores[107], S. Foertsch[68], I. Fokin[93], S. Fokin[140], U. Follo[IV,56], E. Fragiacomo[57], E. Frajna[46], U. Fuchs[32], N. Funicello[28], C. Furget[72], A. Furs[140], T. Fusayasu[97], J.J. Gaardhøje[82], M. Gagliardi[24], A.M. Gago[100], T. Gahlaut[47], C.D. Galvan[108], S. Gami[79], D.R. Gangadharan[115], P. Ganoti[77], C. Garabatos[96], J.M. Garcia[44], T. García Chávez[44], E. Garcia-Solis[9], C. Gargiulo[32], P. Gasik[96], H.M. Gaur[38], A. Gautam[117], M.B. Gay Ducati[66], M. Germain[102], R.A. Gernhaeuser[94], C. Ghosh[134], M. Giacalone[51], G. Gioachin[29], S.K. Giri[134], P. Giubellino[96,56], P. Giubilato[27], A.M.C. Glaenzer[129], P. Glässel[93], E. Glimos[121], D.J.Q. Goh[75], V. Gonzalez[136], P. Gordeev[140], M. Gorgon[2], K. Goswami[48], S. Gotovac[33], V. Grabski[67], L.K. Graczykowski[135], E. Grecka[85], A. Grelli[59], C. Grigoras[32], V. Grigoriev[140], S. Grigoryan[141,1],

F. Grosa[32], J.F. Grosse-Oetringhaus[32], R. Grosso[96], D. Grund[34], N.A. Grunwald[93],
G.G. Guardiano[110], R. Guernane[72], M. Guilbaud[102], K. Gulbrandsen[82], J.J.W.K. Gumprecht[101],
T. Gündem[64], T. Gunji[123], W. Guo[6], A. Gupta[90], R. Gupta[90], R. Gupta[48], K. Gwizdziel[135],
L. Gyulai[46], C. Hadjidakis[130], F.U. Haider[90], S. Haidlova[34], M. Haldar[4], H. Hamagaki[75],
Y. Han[139], B.G. Hanley[136], R. Hannigan[107], J. Hansen[74], M.R. Haque[96], J.W. Harris[137],
A. Harton[9], M.V. Hartung[64], H. Hassan[116], D. Hatzifotiadou[51], P. Hauer[42], L.B. Havener[137],
E. Hellbär[32], H. Helstrup[37], M. Hemmer[64], T. Herman[34], S.G. Hernandez[115], G. Herrera Corral[8],
S. Herrmann[127], K.F. Hetland[37], B. Heybeck[64], H. Hillemanns[32], B. Hippolyte[128], I.P.M. Hobus[83],
F.W. Hoffmann[70], B. Hofman[59], M. Horst[94], A. Horzyk[2], Y. Hou[6], P. Hristov[32], P. Huhn[64],
L.M. Huhta[116], T.J. Humanic[87], A. Hutson[115], D. Hutter[38], M.C. Hwang[18], R. Ilkaev[140],
M. Inaba[124], G.M. Innocenti[32], M. Ippolitov[140], A. Isakov[83], T. Isidori[117], M.S. Islam[47,98],
S. Iurchenko[140], M. Ivanov[13], M. Ivanov[96], V. Ivanov[140], K.E. Iversen[74], M. Jablonski[2],
B. Jacak[18,73], N. Jacazio[25], P.M. Jacobs[73], S. Jadlovska[105], J. Jadlovsky[105], S. Jaelani[81], C. Jahnke[109],
M.J. Jakubowska[135], M.A. Janik[135], T. Janson[70], S. Ji[16], S. Jia[10], T. Jiang[10], A.A.P. Jimenez[65],
F. Jonas[73], D.M. Jones[118], J.M. Jowett[32,96], J. Jung[64], M. Jung[64], A. Junique[32], A. Jusko[99],
J. Kaewjai[104], P. Kalinak[60], A. Kalweit[32], A. Karasu Uysal[V,138], D. Karatovic[88], N. Karatzenis[99],
O. Karavichev[140], T. Karavicheva[140], E. Karpechev[140], M.J. Karwowska[135], U. Kebschull[70],
M. Keil[32], B. Ketzer[42], J. Keul[64], S.S. Khade[48], A.M. Khan[119], S. Khan[15], A. Khanzadeev[140],
Y. Kharlov[140], A. Khatun[117], A. Khuntia[34], Z. Khuranova[64], B. Kileng[37], B. Kim[103], C. Kim[16],
D.J. Kim[116], D. Kim[103], E.J. Kim[69], J. Kim[139], J. Kim[58], J. Kim[32,69], M. Kim[18], S. Kim[17],
T. Kim[139], K. Kimura[91], A. Kirkova[35], S. Kirsch[64], I. Kisel[38], S. Kiselev[140], A. Kisiel[135],
J.L. Klay[5], J. Klein[32], S. Klein[73], C. Klein-Bösing[125], M. Kleiner[64], T. Klemenz[94], A. Kluge[32],
C. Kobdaj[104], R. Kohara[123], T. Kollegger[96], A. Kondratyev[141], N. Kondratyeva[140], J. Konig[64],
S.A. Konigstorfer[94], P.J. Konopka[32], G. Kornakov[135], M. Korwieser[94], S.D. Koryciak[2], C. Koster[83],
A. Kotliarov[85], N. Kovacic[88], V. Kovalenko[140], M. Kowalski[106], V. Kozhuharov[35], G. Kozlov[38],
I. Králik[60], A. Kravčáková[36], L. Krcal[32,38], M. Krivda[99,60], F. Krizek[85], K. Krizkova Gajdosova[32],
C. Krug[66], M. Krüger[64], D.M. Krupova[34], E. Kryshen[140], V. Kučera[58], C. Kuhn[128],
P.G. Kuijer[83], T. Kumaoka[124], D. Kumar[134], L. Kumar[89], N. Kumar[89], S. Kumar[50], S. Kundu[32],
P. Kurashvili[78], A.B. Kurepin[140], A. Kuryakin[140], S. Kushpil[85], V. Kuskov[140], M. Kutyla[135],
A. Kuznetsov[141], M.J. Kweon[58], Y. Kwon[139], S.L. La Pointe[38], P. La Rocca[26], A. Lakrathok[104],
M. Lamanna[32], A.R. Landou[72], R. Langoy[120], P. Larionov[32], E. Laudi[32], L. Lautner[94],
R.A.N. Laveaga[108], R. Lavicka[101], R. Lea[133,55], H. Lee[103], I. Legrand[45], G. Legras[125],
J. Lehrbach[38], A.M. Lejeune[34], T.M. Lelek[2], R.C. Lemmon[I,84], I. León Monzón[108], M.M. Lesch[94],
E.D. Lesser[18], P. Lévai[46], M. Li[6], P. Li[10], X. Li[10], B.E. Liang-gilman[18], J. Lien[120], R. Lietava[99],
I. Likmeta[115], B. Lim[24], H. Lim[16], S.H. Lim[16], V. Lindenstruth[38], C. Lippmann[96], D. Liskova[105],
D.H. Liu[6], J. Liu[118], G.S.S. Liveraro[110], I.M. Lofnes[20], C. Loizides[86], S. Lokos[106], J. Lömker[59],
X. Lopez[126], E. López Torres[7], C. Lotteau[127], P. Lu[96,119], Z. Lu[10], F.V. Lugo[67], J.R. Luhder[125],
G. Luparello[57], Y.G. Ma[39], M. Mager[32], A. Maire[128], E.M. Majerz[2], M.V. Makariev[35],
M. Malaev[140], G. Malfattore[25], N.M. Malik[90], S.K. Malik[90], D. Mallick[130], N. Mallick[116,48],
G. Mandaglio[30,53], S.K. Mandal[78], A. Manea[63], V. Manko[140], F. Manso[126], V. Manzari[50],
Y. Mao[6], R.W. Marcjan[2], G.V. Margagliotti[23], A. Margotti[51], A. Marín[96], C. Markert[107],
C.F.B. Marquez[31], P. Martinengo[32], M.I. Martínez[44], G. Martínez García[102], M.P.P. Martins[109],
S. Masciocchi[96], M. Masera[24], A. Masoni[52], L. Massacrier[130], O. Massen[59], A. Mastroserio[131,50],
S. Mattiazzo[27], A. Matyja[106], F. Mazzaschi[32,24], M. Mazzilli[115], Y. Melikyan[43], M. Melo[109],
A. Menchaca-Rocha[67], J.E.M. Mendez[65], E. Meninno[101], A.S. Menon[115], M.W. Menzel[32,93],
M. Meres[13], L. Micheletti[32], D. Mihai[112], D.L. Mihaylov[94], K. Mikhaylov[141,140], N. Minafra[117],
D. Miśkowiec[96], A. Modak[133], B. Mohanty[79], M. Mohisin Khan[VI,15], M.A. Molander[43],
M.M. Mondal[79], S. Monira[135], C. Mordasini[116], D.A. Moreira De Godoy[125], I. Morozov[140],
A. Morsch[32], T. Mrnjavac[32], V. Muccifora[49], S. Muhuri[134], J.D. Mulligan[73], A. Mulliri[22],
M.G. Munhoz[109], R.H. Munzer[64], H. Murakami[123], S. Murray[113], L. Musa[32], J. Musinsky[60],
J.W. Myrcha[135], B. Naik[122], A.I. Nambrath[18], B.K. Nandi[47], R. Nania[51], E. Nappi[50],
A.F. Nassirpour[17], V. Nastase[112], A. Nath[93], S. Nath[134], C. Nattrass[121], T.K. Nayak[115],
M.N. Naydenov[35], A. Neagu[19], A. Negru[112], E. Nekrasova[140], L. Nellen[65], R. Nepeivoda[74], S. Nese[19],
N. Nicassio[50], B.S. Nielsen[82], E.G. Nielsen[82], S. Nikolaev[140], S. Nikulin[140], V. Nikulin[140],
F. Noferini[51], S. Noh[12], P. Nomokonov[141], J. Norman[118], N. Novitzky[86], P. Nowakowski[135],
A. Nyanin[140], J. Nystrand[20], S. Oh[17], A. Ohlson[74], V.A. Okorokov[140], J. Oleniacz[135],

A. Onnerstad[116], C. Oppedisano[56], A. Ortiz Velasquez[65], J. Otwinowski[106], M. Oya[91], K. Oyama[75], S. Padhan[47], D. Pagano[133,55], G. Paić[65], S. Paisano-Guzmán[44], A. Palasciano[50], I. Panasenko[74], S. Panebianco[129], C. Pantouvakis[27], H. Park[124], J. Park[124], S. Park[103], J.E. Parkkila[32], Y. Patley[47], R.N. Patra[50], B. Paul[134], H. Pei[6], T. Peitzmann[59], X. Peng[11], M. Pennisi[24], S. Perciballi[24], D. Peresunko[140], G.M. Perez[7], Y. Pestov[140], M.T. Petersen[82], V. Petrov[140], M. Petrovici[45], S. Piano[57], M. Pikna[13], P. Pillot[102], O. Pinazza[51,32], L. Pinsky[115], C. Pinto[94], S. Pisano[49], M. Płoskoń[73], M. Planinic[88], D.K. Plociennik[2], M.G. Poghosyan[86], B. Polichtchouk[140], S. Politano[29], N. Poljak[88], A. Pop[45], S. Porteboeuf-Houssais[126], V. Pozdniakov[I,141], I.Y. Pozos[44], K.K. Pradhan[48], S.K. Prasad[4], S. Prasad[48], R. Preghenella[51], F. Prino[56], C.A. Pruneau[136], I. Pshenichnov[140], M. Puccio[32], S. Pucillo[24], S. Qiu[83], L. Quaglia[24], A.M.K. Radhakrishnan[48], S. Ragoni[14], A. Rai[137], A. Rakotozafindrabe[129], L. Ramello[132,56], M. Rasa[26], S.S. Räsänen[43], R. Rath[51], M.P. Rauch[20], I. Ravasenga[32], K.F. Read[86,121], C. Reckziegel[111], A.R. Redelbach[38], K. Redlich[VII,78], C.A. Reetz[96], H.D. Regules-Medel[44], A. Rehman[20], F. Reidt[32], H.A. Reme-Ness[37], K. Reygers[93], A. Riabov[140], V. Riabov[140], R. Ricci[28], M. Richter[20], A.A. Riedel[94], W. Riegler[32], A.G. Riffero[24], M. Rignanese[27], C. Ripoli[28], C. Ristea[63], M.V. Rodriguez[32], M. Rodríguez Cahuantzi[44], S.A. Rodríguez Ramírez[44], K. Røed[19], R. Rogalev[140], E. Rogochaya[141], T.S. Rogoschinski[64], D. Rohr[32], D. Röhrich[20], S. Rojas Torres[34], P.S. Rokita[135], G. Romanenko[25], F. Ronchetti[32], E.D. Rosas[65], K. Roslon[135], A. Rossi[54], A. Roy[48], S. Roy[47], N. Rubini[51,25], J.A. Rudolph[83], D. Ruggiano[135], R. Rui[23], P.G. Russek[2], R. Russo[83], A. Rustamov[80], E. Ryabinkin[140], Y. Ryabov[140], A. Rybicki[106], J. Ryu[16], W. Rzesa[135], B. Sabiu[51], S. Sadovsky[140], J. Saetre[20], S. Saha[79], B. Sahoo[47], B. Sahoo[48], R. Sahoo[48], S. Sahoo[61], D. Sahu[48], P.K. Sahu[61], J. Saini[134], K. Sajdakova[36], S. Sakai[124], M.P. Salvan[96], S. Sambyal[90], D. Samitz[101], I. Sanna[32,94], T.B. Saramela[109], D. Sarkar[82], P. Sarma[41], V. Sarritzu[22], V.M. Sarti[94], M.H.P. Sas[32], S. Sawan[79], E. Scapparone[51], J. Schambach[86], H.S. Scheid[64], C. Schiaua[45], R. Schicker[93], F. Schlepper[93], A. Schmah[96], C. Schmidt[96], M.O. Schmidt[32], M. Schmidt[92], N.V. Schmidt[86], A.R. Schmier[121], R. Schotter[101,128], A. Schröter[38], J. Schukraft[32], K. Schweda[96], G. Scioli[25], E. Scomparin[56], J.E. Seger[14], Y. Sekiguchi[123], D. Sekihata[123], M. Selina[83], I. Selyuzhenkov[96], S. Senyukov[128], J.J. Seo[93], D. Serebryakov[140], L. Serkin[VIII,65], L. Šerkšnytė[94], A. Sevcenco[63], T.J. Shaba[68], A. Shabetai[102], R. Shahoyan[32], A. Shangaraev[140], B. Sharma[90], D. Sharma[47], H. Sharma[54], M. Sharma[90], S. Sharma[75], S. Sharma[90], U. Sharma[90], A. Shatat[130], O. Sheibani[136,115], K. Shigaki[91], M. Shimomura[76], J. Shin[12], S. Shirinkin[140], Q. Shou[39], Y. Sibiriak[140], S. Siddhanta[52], T. Siemiarczuk[78], T.F. Silva[109], D. Silvermyr[74], T. Simantathammakul[104], R. Simeonov[35], B. Singh[90], B. Singh[94], K. Singh[48], R. Singh[79], R. Singh[90], R. Singh[54,96], S. Singh[15], V.K. Singh[134], V. Singhal[134], T. Sinha[98], B. Sitar[13], M. Sitta[132,56], T.B. Skaali[19], G. Skorodumovs[93], N. Smirnov[137], R.J.M. Snellings[59], E.H. Solheim[19], C. Sonnabend[32,96], J.M. Sonneveld[83], F. Soramel[27], A.B. Soto-hernandez[87], R. Spijkers[83], I. Sputowska[106], J. Staa[74], J. Stachel[93], I. Stan[63], P.J. Steffanic[121], T. Stellhorn[125], S.F. Stiefelmaier[93], D. Stocco[102], I. Storehaug[19], N.J. Strangmann[64], P. Stratmann[125], S. Strazzi[25], A. Sturniolo[30,53], C.P. Stylianidis[83], A.A.P. Suaide[109], C. Suire[130], A. Suiu[32,112], M. Sukhanov[140], M. Suljic[32], R. Sultanov[140], V. Sumberia[90], S. Sumowidagdo[81], M. Szymkowski[135], L.H. Tabares[7], S.F. Taghavi[94], J. Takahashi[110], G.J. Tambave[79], S. Tang[6], Z. Tang[119], J.D. Tapia Takaki[117], N. Tapus[112], L.A. Tarasovicova[36], M.G. Tarzila[45], A. Tauro[32], A. Tavira García[130], G. Tejeda Muñoz[44], L. Terlizzi[24], C. Terrevoli[50], S. Thakur[4], M. Thogersen[19], D. Thomas[107], A. Tikhonov[140], N. Tiltmann[32,125], A.R. Timmins[115], M. Tkacik[105], T. Tkacik[105], A. Toia[64], R. Tokumoto[91], S. Tomassini[25], K. Tomohiro[91], N. Topilskaya[140], M. Toppi[49], V.V. Torres[102], A.G. Torres Ramos[31], A. Trifiró[30,53], T. Triloki[95], A.S. Triolo[32,30,53], S. Tripathy[32], T. Tripathy[47], S. Trogolo[24], V. Trubnikov[3], W.H. Trzaska[116], T.P. Trzcinski[135], C. Tsolanta[19], R. Tu[39], A. Tumkin[140], R. Turrisi[54], T.S. Tveter[19], K. Ullaland[20], B. Ulukutlu[94], S. Upadhyaya[106], A. Uras[127], G.L. Usai[22], M. Vala[36], N. Valle[55], L.V.R. van Doremalen[59], M. van Leeuwen[83], C.A. van Veen[93], R.J.G. van Weelden[83], P. Vande Vyvre[32], D. Varga[46], Z. Varga[137,46], P. Vargas Torres[65], M. Vasileiou[77], A. Vasiliev[I,140], O. Vázquez Doce[49], O. Vazquez Rueda[115], V. Vechernin[140], E. Vercellin[24], R. Verma[47], R. Vértesi[46], M. Verweij[59], L. Vickovic[33], Z. Vilakazi[122], O. Villalobos Baillie[99], A. Villani[23], A. Vinogradov[140], T. Virgili[28], M.M.O. Virta[116], A. Vodopyanov[141], B. Volkel[32], M.A. Völkl[93], S.A. Voloshin[136], G. Volpe[31], B. von Haller[32], I. Vorobyev[32], N. Vozniuk[140], J. Vrláková[36], J. Wan[39], C. Wang[39], D. Wang[39], Y. Wang[39], Y. Wang[6], Z. Wang[39], A. Wegrzynek[32], F.T. Weiglhofer[38], S.C. Wenzel[32], J.P. Wessels[125], P.K. Wiacek[2], J. Wiechula[64], J. Wikne[19],

G. Wilk[78], J. Wilkinson[96], G.A. Willems[125], B. Windelband[93], M. Winn[129], J.R. Wright[107], W. Wu[39], Y. Wu[119], Z. Xiong[119], R. Xu[6], A. Yadav[42], A.K. Yadav[134], Y. Yamaguchi[91], S. Yang[20], S. Yano[91], E.R. Yeats[18], Z. Yin[6], I.-K. Yoo[16], J.H. Yoon[58], H. Yu[12], S. Yuan[20], A. Yuncu[93], V. Zaccolo[23], C. Zampolli[32], F. Zanone[93], N. Zardoshti[32], A. Zarochentsev[140], P. Závada[62], N. Zaviyalov[140], M. Zhalov[140], B. Zhang[93,6], C. Zhang[129], L. Zhang[39], M. Zhang[126,6], M. Zhang[6], S. Zhang[39], X. Zhang[6], Y. Zhang[119], Z. Zhang[6], M. Zhao[10], V. Zherebchevskii[140], Y. Zhi[10], D. Zhou[6], Y. Zhou[82], J. Zhu[54,6], S. Zhu[119], Y. Zhu[6], S.C. Zugravel[56], N. Zurlo[133,55]

Affiliation Notes

[I] Deceased
[II] Also at: Max-Planck-Institut fur Physik, Munich, Germany
[III] Also at: Italian National Agency for New Technologies, Energy and Sustainable Economic Development (ENEA), Bologna, Italy
[IV] Also at: Dipartimento DET del Politecnico di Torino, Turin, Italy
[V] Also at: Yildiz Technical University, Istanbul, Türkiye
[VI] Also at: Department of Applied Physics, Aligarh Muslim University, Aligarh, India
[VII] Also at: Institute of Theoretical Physics, University of Wroclaw, Poland
[VIII] Also at: Facultad de Ciencias, Universidad Nacional Autónoma de México, Mexico City, Mexico
[IX] Also at: An institution covered by a cooperation agreement with CERN

Collaboration Institutes

[1] A.I. Alikhanyan National Science Laboratory (Yerevan Physics Institute) Foundation, Yerevan, Armenia
[2] AGH University of Krakow, Cracow, Poland
[3] Bogolyubov Institute for Theoretical Physics, National Academy of Sciences of Ukraine, Kiev, Ukraine
[4] Bose Institute, Department of Physics and Centre for Astroparticle Physics and Space Science (CAPSS), Kolkata, India
[5] California Polytechnic State University, San Luis Obispo, California, United States
[6] Central China Normal University, Wuhan, China
[7] Centro de Aplicaciones Tecnológicas y Desarrollo Nuclear (CEADEN), Havana, Cuba
[8] Centro de Investigación y de Estudios Avanzados (CINVESTAV), Mexico City and Mérida, Mexico
[9] Chicago State University, Chicago, Illinois, United States
[10] China Institute of Atomic Energy, Beijing, China
[11] China University of Geosciences, Wuhan, China
[12] Chungbuk National University, Cheongju, Republic of Korea
[13] Comenius University Bratislava, Faculty of Mathematics, Physics and Informatics, Bratislava, Slovak Republic
[14] Creighton University, Omaha, Nebraska, United States
[15] Department of Physics, Aligarh Muslim University, Aligarh, India
[16] Department of Physics, Pusan National University, Pusan, Republic of Korea
[17] Department of Physics, Sejong University, Seoul, Republic of Korea
[18] Department of Physics, University of California, Berkeley, California, United States
[19] Department of Physics, University of Oslo, Oslo, Norway
[20] Department of Physics and Technology, University of Bergen, Bergen, Norway
[21] Dipartimento di Fisica, Università di Pavia, Pavia, Italy
[22] Dipartimento di Fisica dell'Università and Sezione INFN, Cagliari, Italy
[23] Dipartimento di Fisica dell'Università and Sezione INFN, Trieste, Italy
[24] Dipartimento di Fisica dell'Università and Sezione INFN, Turin, Italy
[25] Dipartimento di Fisica e Astronomia dell'Università and Sezione INFN, Bologna, Italy
[26] Dipartimento di Fisica e Astronomia dell'Università and Sezione INFN, Catania, Italy
[27] Dipartimento di Fisica e Astronomia dell'Università and Sezione INFN, Padova, Italy
[28] Dipartimento di Fisica 'E.R. Caianiello' dell'Università and Gruppo Collegato INFN, Salerno, Italy
[29] Dipartimento DISAT del Politecnico and Sezione INFN, Turin, Italy
[30] Dipartimento di Scienze MIFT, Università di Messina, Messina, Italy
[31] Dipartimento Interateneo di Fisica 'M. Merlin' and Sezione INFN, Bari, Italy
[32] European Organization for Nuclear Research (CERN), Geneva, Switzerland

[33] Faculty of Electrical Engineering, Mechanical Engineering and Naval Architecture, University of Split, Split, Croatia
[34] Faculty of Nuclear Sciences and Physical Engineering, Czech Technical University in Prague, Prague, Czech Republic
[35] Faculty of Physics, Sofia University, Sofia, Bulgaria
[36] Faculty of Science, P.J. Šafárik University, Košice, Slovak Republic
[37] Faculty of Technology, Environmental and Social Sciences, Bergen, Norway
[38] Frankfurt Institute for Advanced Studies, Johann Wolfgang Goethe-Universität Frankfurt, Frankfurt, Germany
[39] Fudan University, Shanghai, China
[40] Gangneung-Wonju National University, Gangneung, Republic of Korea
[41] Gauhati University, Department of Physics, Guwahati, India
[42] Helmholtz-Institut für Strahlen- und Kernphysik, Rheinische Friedrich-Wilhelms-Universität Bonn, Bonn, Germany
[43] Helsinki Institute of Physics (HIP), Helsinki, Finland
[44] High Energy Physics Group, Universidad Autónoma de Puebla, Puebla, Mexico
[45] Horia Hulubei National Institute of Physics and Nuclear Engineering, Bucharest, Romania
[46] HUN-REN Wigner Research Centre for Physics, Budapest, Hungary
[47] Indian Institute of Technology Bombay (IIT), Mumbai, India
[48] Indian Institute of Technology Indore, Indore, India
[49] INFN, Laboratori Nazionali di Frascati, Frascati, Italy
[50] INFN, Sezione di Bari, Bari, Italy
[51] INFN, Sezione di Bologna, Bologna, Italy
[52] INFN, Sezione di Cagliari, Cagliari, Italy
[53] INFN, Sezione di Catania, Catania, Italy
[54] INFN, Sezione di Padova, Padova, Italy
[55] INFN, Sezione di Pavia, Pavia, Italy
[56] INFN, Sezione di Torino, Turin, Italy
[57] INFN, Sezione di Trieste, Trieste, Italy
[58] Inha University, Incheon, Republic of Korea
[59] Institute for Gravitational and Subatomic Physics (GRASP), Utrecht University/Nikhef, Utrecht, Netherlands
[60] Institute of Experimental Physics, Slovak Academy of Sciences, Košice, Slovak Republic
[61] Institute of Physics, Homi Bhabha National Institute, Bhubaneswar, India
[62] Institute of Physics of the Czech Academy of Sciences, Prague, Czech Republic
[63] Institute of Space Science (ISS), Bucharest, Romania
[64] Institut für Kernphysik, Johann Wolfgang Goethe-Universität Frankfurt, Frankfurt, Germany
[65] Instituto de Ciencias Nucleares, Universidad Nacional Autónoma de México, Mexico City, Mexico
[66] Instituto de Física, Universidade Federal do Rio Grande do Sul (UFRGS), Porto Alegre, Brazil
[67] Instituto de Física, Universidad Nacional Autónoma de México, Mexico City, Mexico
[68] iThemba LABS, National Research Foundation, Somerset West, South Africa
[69] Jeonbuk National University, Jeonju, Republic of Korea
[70] Johann-Wolfgang-Goethe Universität Frankfurt Institut für Informatik, Fachbereich Informatik und Mathematik, Frankfurt, Germany
[71] Korea Institute of Science and Technology Information, Daejeon, Republic of Korea
[72] Laboratoire de Physique Subatomique et de Cosmologie, Université Grenoble-Alpes, CNRS-IN2P3, Grenoble, France
[73] Lawrence Berkeley National Laboratory, Berkeley, California, United States
[74] Lund University Department of Physics, Division of Particle Physics, Lund, Sweden
[75] Nagasaki Institute of Applied Science, Nagasaki, Japan
[76] Nara Women's University (NWU), Nara, Japan
[77] National and Kapodistrian University of Athens, School of Science, Department of Physics , Athens, Greece
[78] National Centre for Nuclear Research, Warsaw, Poland
[79] National Institute of Science Education and Research, Homi Bhabha National Institute, Jatni, India
[80] National Nuclear Research Center, Baku, Azerbaijan
[81] National Research and Innovation Agency - BRIN, Jakarta, Indonesia
[82] Niels Bohr Institute, University of Copenhagen, Copenhagen, Denmark
[83] Nikhef, National institute for subatomic physics, Amsterdam, Netherlands

[84] Nuclear Physics Group, STFC Daresbury Laboratory, Daresbury, United Kingdom
[85] Nuclear Physics Institute of the Czech Academy of Sciences, Husinec-Řež, Czech Republic
[86] Oak Ridge National Laboratory, Oak Ridge, Tennessee, United States
[87] Ohio State University, Columbus, Ohio, United States
[88] Physics department, Faculty of science, University of Zagreb, Zagreb, Croatia
[89] Physics Department, Panjab University, Chandigarh, India
[90] Physics Department, University of Jammu, Jammu, India
[91] Physics Program and International Institute for Sustainability with Knotted Chiral Meta Matter (WPI-SKCM^2), Hiroshima University, Hiroshima, Japan
[92] Physikalisches Institut, Eberhard-Karls-Universität Tübingen, Tübingen, Germany
[93] Physikalisches Institut, Ruprecht-Karls-Universität Heidelberg, Heidelberg, Germany
[94] Physik Department, Technische Universität München, Munich, Germany
[95] Politecnico di Bari and Sezione INFN, Bari, Italy
[96] Research Division and ExtreMe Matter Institute EMMI, GSI Helmholtzzentrum für Schwerionenforschung GmbH, Darmstadt, Germany
[97] Saga University, Saga, Japan
[98] Saha Institute of Nuclear Physics, Homi Bhabha National Institute, Kolkata, India
[99] School of Physics and Astronomy, University of Birmingham, Birmingham, United Kingdom
[100] Sección Física, Departamento de Ciencias, Pontificia Universidad Católica del Perú, Lima, Peru
[101] Stefan Meyer Institut für Subatomare Physik (SMI), Vienna, Austria
[102] SUBATECH, IMT Atlantique, Nantes Université, CNRS-IN2P3, Nantes, France
[103] Sungkyunkwan University, Suwon City, Republic of Korea
[104] Suranaree University of Technology, Nakhon Ratchasima, Thailand
[105] Technical University of Košice, Košice, Slovak Republic
[106] The Henryk Niewodniczanski Institute of Nuclear Physics, Polish Academy of Sciences, Cracow, Poland
[107] The University of Texas at Austin, Austin, Texas, United States
[108] Universidad Autónoma de Sinaloa, Culiacán, Mexico
[109] Universidade de São Paulo (USP), São Paulo, Brazil
[110] Universidade Estadual de Campinas (UNICAMP), Campinas, Brazil
[111] Universidade Federal do ABC, Santo Andre, Brazil
[112] Universitatea Nationala de Stiinta si Tehnologie Politehnica Bucuresti, Bucharest, Romania
[113] University of Cape Town, Cape Town, South Africa
[114] University of Derby, Derby, United Kingdom
[115] University of Houston, Houston, Texas, United States
[116] University of Jyväskylä, Jyväskylä, Finland
[117] University of Kansas, Lawrence, Kansas, United States
[118] University of Liverpool, Liverpool, United Kingdom
[119] University of Science and Technology of China, Hefei, China
[120] University of South-Eastern Norway, Kongsberg, Norway
[121] University of Tennessee, Knoxville, Tennessee, United States
[122] University of the Witwatersrand, Johannesburg, South Africa
[123] University of Tokyo, Tokyo, Japan
[124] University of Tsukuba, Tsukuba, Japan
[125] Universität Münster, Institut für Kernphysik, Münster, Germany
[126] Université Clermont Auvergne, CNRS/IN2P3, LPC, Clermont-Ferrand, France
[127] Université de Lyon, CNRS/IN2P3, Institut de Physique des 2 Infinis de Lyon, Lyon, France
[128] Université de Strasbourg, CNRS, IPHC UMR 7178, F-67000 Strasbourg, France, Strasbourg, France
[129] Université Paris-Saclay, Centre d'Etudes de Saclay (CEA), IRFU, Départment de Physique Nucléaire (DPhN), Saclay, France
[130] Université Paris-Saclay, CNRS/IN2P3, IJCLab, Orsay, France
[131] Università degli Studi di Foggia, Foggia, Italy
[132] Università del Piemonte Orientale, Vercelli, Italy
[133] Università di Brescia, Brescia, Italy
[134] Variable Energy Cyclotron Centre, Homi Bhabha National Institute, Kolkata, India
[135] Warsaw University of Technology, Warsaw, Poland
[136] Wayne State University, Detroit, Michigan, United States

[137] Yale University, New Haven, Connecticut, United States
[138] Yildiz Technical University, Istanbul, Turkey
[139] Yonsei University, Seoul, Republic of Korea
[140] Affiliated with an institute covered by a cooperation agreement with CERN
[141] Affiliated with an international laboratory covered by a cooperation agreement with CERN.